AN ABSTRACT OF THE THESIS OF

Helmut P. Frank for the degree of Master of Science in Atmospheric Sciences presented on April 3, 1986.

Title: Turbulent Structure in the Bora and Stable Boundary Layer

Abstract approved: Redacted for Privacy

Larry Mahrt

An eigenvector analysis of the velocity-temperature correlation matrix is applied to clear-air turbulence measured by aircraft in the Bora. The eigenvectors are identified with the main eddies of the turbulence. This study attempts to infer the three-dimensional structure of these eddies. The results are compared with turbulent structures in the stable boundary layer. The turbulence in the strongly stratified boundary layer appears to be dominated by double roller eddies with their axes of rotation tilted in the shear direction. The clear-air turbulence shows a larger variety of motion types.

# TURBULENT STRUCTURE IN THE BORA AND STABLE BOUNDARY LAYER

by

Helmut P. Frank

A THESIS

submitted to

Oregon State Unversity

in partial fulfullment of
the requirements for the
degree of

Master of Science

Completed April 3, 1986

Commencement June 1986

APPROVED:

Redacted for Privacy

Professor of Atmospheric Science in Charge of Major

Redacted for Privacy

Head of Department of Atmospheric Sciences

Redacted for Privacy

Dean of Graduate School

Date thesis is presented April 3, 1986

Typed by Michelle Holcomb for Helmut P. Frank

## Acknowledgements

I am deeply indebted to Professor Larry Mahrt for his guidance and advise for this work. Also, I want to thank Professors J. Deardorff and T. Dillon for their comments on the final form of the thesis. The advice on the use of the computers and the graphics devices by Wayne Gibson and William McKie is greatly appreciated. Appreciation is also due to the OSU Climatic Research Institute and the National Center for Atmospheric Research for computer resources. Thanks to Michelle Holcomb for typing and re-typing the thesis.

This study was supported in the form of a graduate research assistantship by the Meteorology Program and Global Atmospheric Research Program of the National Science Foundation through Grants ATM 8306141 and ATM 8306874.

Table of Contents

## List of Figures

List of Tables

# TURBULENT STRUCTURE IN THE BORA AND STABLE BOUNDARY LAYER

## 1. Introduction

Turbulent flows are very chaotic, and at first glance appear devoid of definable structures. But, since we believe that the equations for fluid motion, in particular the Navier-Stokes equations, are relatively accurate looking for structures becomes more promising. These equations put constraints on the motion so that turbulent quantities cannot take totally random values. The structures of the flow might be quite important for the turbulent transport of momentum, heat or other scalars such as pollutants.

It is assumed that the coherent structures make up the main part of the turbulent motion. Therefore, they are called the main eddies. They are assumed to be relatively uniform for a wide range of turbulent motions (Townsend, 1976). Townsend tried to qualitatively infer their structure from the velocity correlation matrix. Lumley (1965) proposed an analytical way to find the main eddies. He proposed that they were the eigenvectors of the correlation matrix corresponding to the largest eigenvalues. The main eddy is the eigenvector which explains most of the variance of the flow, (i.e., the first eigenvector corresponds to the largest eigenvalue).

Payne and Lumley (1967) applied the method to measurements in the wake of a cylinder by Grant (1958). They found a double roller eddy which leaned slightly against the mean shear direction. Petersen (1976) used eigenvectors of a time-laged velocity correlation matrix to simulate turbulent gusts.

In other areas of meteorology the eigenvectors of a correlation matrix are sometimes called empirical orthogonal functions. They were used, for example, by Lorenz (1956) and Kutzbach (1967). Kutzbach tried a physical interpretation of eigenvectors of sea level pressure, surface temperature, and precipitation complexes over North America.

This study will apply an eigenvector analysis to the velocity and temperature data collected by aircraft over the Yugoslavian coast during "The Alpine Experiment" (ALPEX) in March 1982. Therefore, the measurements are along a line and the full three dimensional structure of events can be inferred only tentatively from the velocity field.

In Chapter 2 the theory of orthogonal decomposition of random functions is explained. Chapter 3 shows model calculations for statistically homogeneous functions. Chapter 4 contains the analysis of the ALPEX data, and Chapter 5 compares this analysis briefly with an analysis of boundary layer turbulence.

## 2. Empirical Orthogonal Functions

The development will follow mainly that of Dutton (1969) and Busch and Petersen (1971).

Suppose we have an ensemble of functions $f_n(x)$ on a finite domain, $a \leq x \leq b$. We want to find a function $\phi$ that is simultaneously similar to all functions $f_n$ in some sense. As a measure of similarity, $\rho^2$, we choose the square of the scalar product between $f_n$ and $\phi$ normalized by the magnitude of $\phi$.

$$\rho^2 = \frac{\left(\int_a^b f_n \phi dx\right)^2}{\int_a^b \phi^2 dx} \tag{1}$$

From Schwartz's inequality it follows that

$$0 \leq \frac{\rho^2}{\int f_n^2 dx} = \frac{\rho^2}{|f_n|^2} \leq 1$$

and $\rho^2/|f_n|^2 = 1$ if $\phi = \pm f_n$.

The average similarity between $\phi$ and any function of the ensemble is then

$$\lambda = E\{\rho^2\} = E\left\{\frac{(\int f_n \phi dx)^2}{\int \phi^2 dx}\right\} \tag{2}$$

where E is the expectation operator.

To determine the maximum of $\lambda$ we use techniques of variational calculus. Assume $\lambda$ were maximal for $\phi$. If $\phi$ was perturbed a little bit by $\varepsilon\delta\phi$, then

$$\lambda(\varepsilon) = E\left\{\frac{(\int f_n(\phi + \varepsilon\delta\phi)dx)^2}{\int(\phi + \varepsilon\delta\phi)^2 dx}\right\}$$

and from the assumption $\lambda$ is maximal for $\varepsilon = 0$. Hence, $\phi$ must satisfy the condition

$$\frac{d\lambda(\varepsilon)}{d\varepsilon}\Big|_{\varepsilon=0} = 0$$

Performing the differentiation and setting $\varepsilon = 0$ gives

$$\int \left[\int E\{f_n(x)f_n(y)\}\phi(x)dx - \lambda\phi(y)\right]\delta\phi(y)dy = 0 \qquad (3)$$

where we assumed that $\lambda(\varepsilon)$ is a smooth function so that expectation and differentiation are interchangable. Since (3) must be satisfied for any $\delta\phi(y)$, it follows that

$$\int E\{f_n(x)f_n(y)\}\phi(x)dx = \lambda\phi(y) \qquad (4)$$

$K(x,y) = E\{f_n(x)f_n(y)\}$ is the covariance function and Eq. (4) is an eigenfunction relation.

Discrete Form

If we have N realizations of the discrete functions $f_n(x_i)$, where $x_i = a + i\Delta x$, $x_p = a + p\Delta x = b$, we define

$$\lambda = \frac{1}{N}\sum_{n=1}^{N}\frac{\left[\sum_{i=0}^{p} f_n(x_i)\phi_i\right]^2}{\sum_{i=0}^{p}\phi_i^2}$$

where $\phi_i = \phi(x_i)$.

Calculations analogous to those in the continuous case give

$$\sum_{i=0}^{p} K_{ij}\phi_i = \lambda\phi_j$$

where $K_{ij} = \frac{1}{N}\sum_{n=1}^{N} f_n(x_i)f_n(x_j)$ is the covariance matrix.

Properties of the Eigenfunctions

(i) The covariance function $K(x,y)$ is symmetric in x and y, i.e., $K(x,y) = K(y,x)$. Also, it follows from the definition of $K(x,y)$ that it is non-negative definite.

(ii) We will assume it is continuous if the sample functions are continuous.

(iii) By (ii) $K(x,y)$ is of bounded variation and square integrable on the closed interval $[a,b]$, where it is defined.

If $K(x,y)$ fulfills these conditions, it may be shown that Eq. (4) has the following properties, (Courant and Hilbert, 1968).

1) It has at least one solution and at most an infinite, but enumerable number of solutions, i.e.,

$$\int K(x,y)\phi_k(x)dx = \lambda_k\phi_k(y) \qquad k = 1,2,3,\ldots,N \qquad (5)$$

2) All the eigenvalues are real and non-negative.

3) The eigenfunctions $\phi_k$ are real and orthogonal. Naturally, they can be orthonormalized, and this will be assumed for the following developments.

For the proper orthogonal decomposition we need Mercer's theorem. It states that if a non-negative definite function $K(x,y)$ is continuous on the interval $[a,b]$, and symmetric in x and y, then,

$$K(x,y) = \sum_{k=1}^{N} \lambda_k\phi_k(x)\phi_k^*(y) \qquad (6)$$

where the $\phi_k(x)$ are the eigenfunctions and the $\lambda_k$ eigenvalues of $K(x,y)$ and $\phi_k^*$ is the complex conjugate of $\phi_k$ for generality. The series converges uniformly in x and y.

Proper Orthogonal Decomposition

We can form the scalar product of the ensemble functions $f_n(x)$ and $\phi_k(x)$ to obtain coefficients

$$a_k = \int f_n(x)\phi_k(x)dx \tag{7}$$

Now, the question is whether or not we have enough eigenfunctions, $\phi_k(x)$ to expand $f_n(x)$ in terms of the $\phi_k(x)$, i.e., does the following equation hold?

$$f_n(x) = \sum_{k=1}^{N} a_k\phi_k(x)$$

To answer it we calculate the square of the expected difference. (We shall assume only real valued functions.)

$$J = E\{[f_n(x) - \sum_{k=1}^{N} a_k\phi_k(x)]^2\}$$

$$= E\{f_n(x)f_n(x) - 2\sum_{k=1}^{N} f_n(x)a_k\phi_k(x) + \sum_{k=1}^{N}\sum_{\ell=1}^{N} a_k a_\ell \phi_k(x)\phi_\ell(x)\}$$

$$= K(x,x) - 2\sum_{k=1}^{N} E\{f_n(x)a_k\}\phi_n(x) + \sum_{k=1}^{N}\sum_{\ell=1}^{N} E\{a_k a_\ell\}\phi_k(x)\phi_\ell(x) \tag{8}$$

with Eq. (7) we get

$$E\{f_n(x)a_k\} = E\{\int f_n(x)f_n(y)\phi_k(y)dy\} = \int K(x,y)\phi_k(y)dy$$

$$= \lambda_k\phi_k(x)$$

and

$$E\{a_k a_\ell\} = E\{\int f_n(y)f_n(z)\phi_k(y)dy\ \phi_\ell(z)dz\}$$

$$= \int\int K(y,z)\phi_k(y)dy\ \phi_\ell(z)dz = \lambda_k \int \phi_k(z)\phi_\ell(z)dz$$

$$= \lambda_k\delta_{k\ell} \tag{9}$$

$\delta_{k\ell}$ is the Kronecker symbol which is 1 if $k = \ell$, and 0 if $k \neq \ell$. So, Eq. (8) becomes

$$y = K(x,x) - 2\sum_{k=1}^{N} \lambda_k \phi_k(x)\phi_k(x) + \sum_{k=1}^{N}\sum_{\ell=1}^{N} \lambda_k \delta_{k\ell} \phi_k(x)\phi_\ell(x)$$

$$= K(x,x) - \sum_{k=1}^{N} \lambda_k \phi_k(x)\phi_k(x) = 0$$

where Mercer's theorem [Eq. (6)] was used in the last step.

Thus, we have shown the proper orthogonal decomposition theorem. A random function $f_n(x)$ which is mean-square continuous on an interval [a,b] has a decomposition

$$f_n(x) = \sum_{k=1}^{N} a_k \phi_k(x) \tag{10}$$

with $E\{a_k a_\ell\} = \lambda_k \delta_{k\ell}$, i.e., the expansion coefficients are uncorrelated, and the functions $\phi_k(x)$ are orthonormal, $\int \phi_k(x)\phi_\ell(x)dx = \delta_{k\ell}$, if and only if $\lambda_k$ are the eigenvalues and $\phi_k(x)$ the orthonormal eigenfunctions of the covariance matrix $K(x,y)$.

## Explaining Maximum Variance

The functions $\phi_k(x)$ found above have a structure close to the ensemble of functions $f_n$ in the sense that they are most parallel to all the sample functions; but there might be other goals too. We might want to look for a set of orthonormal functions $\psi_k(x)$ with the property that if the functions $f_n(x)$ are expanded in terms of $\psi_k(k)$, $\psi_1(x)$ explains most of the variance of the $f_n(x)$, $\psi_2$ explains most of the variance not explained by $\psi_i(x)$, and so on, i.e., we want to minimize the quantity

$$E\{e(M)\} = E\{\int [f_n(x) - \sum_{k=1}^{M} b_k\psi_k(x)]^2 dx\}$$

for all M = 1,2,...,N.

In the same way as above, $\psi_k$ must satisfy the equation

$$\frac{dE\{e(M,\varepsilon)\}}{d\varepsilon}\Big|_{\varepsilon=0} = \frac{d}{d\varepsilon} E\{\int [f_n(x) - \sum_{k=1}^{M} (b_k + \varepsilon\delta b_k)(\psi_k(x) + \varepsilon\delta\psi_k(x)]^2 dx\}\Big|_{\varepsilon=0} = 0 \qquad (11)$$

Using the orthonormality of the functions $\psi_k(x)$, and

$$b_k + \varepsilon\delta b_k = \int f_n(y)[\psi_k(y) + \varepsilon\delta\psi_k(y)]dy ,$$

and that Eq. (11) must hold for any N and $\delta\psi_k$, it can be simplified to

$$\int K(x,y)\psi_k(y)dy = \sum_{\ell=1}^{M} E\{b_k b_\ell\}\psi_\ell(x), \qquad k \leq M \qquad (12)$$

For M = 1, Eq. (12) becomes

$$\int K(x,y)\psi_1(y)dy = E\{b_1^2\}\psi_1(x)$$

this is equivalent to Eq. (5), so

$$\psi_1(x) = \phi_1(x) \quad \text{and} \quad E\{b_1^2\} = \lambda_1 = E\{a_1^2\}$$

For M = 2, Eq. (12) becomes

$$\int K(x,y)\psi_1(y)dy = E\{b_1^2\}\psi_1(x) + E\{b_1 b_2\}\psi_2(x)$$

$$\int K(x,y)\psi_2(y)dy = E\{b_1 b_2\}\psi_2(x) + E\{b_2^2\}\psi_2(x)$$

From this follows

$$E\{b_1 b_2\} = 0, \quad E\{b_2^2\} = \lambda_2, \quad \psi_2(x) = \phi_2(x)$$

In the same way it follows for all k

$$E\{b_k b_\ell\} = \lambda_k \delta_{k\ell}$$

and

$$\psi_k(x) = \phi_k(x)$$

This shows that the eigenfunctions $\phi_k(x)$, which are most similar to the sample functions $f_n(x)$, also explain most of the variance of these functions if we terminate the expansion of $f_n(x)$ in $\phi_k(x)$ after any M functions. The eigenvalues $\lambda_k$ give the variance explained by the $\phi_k$ and in the future, the eigenfunctions $\phi_1$, $\phi_2$, $\phi_3$, ... will be ordered such that $\lambda_1 \geq \lambda_2 \geq \lambda_3 \geq \ldots$

Homogeneous Ensemble

The covariance function of a statistically homogeneous record is a function only of the difference of x and y, i.e.,

$$K(x,y) = K(x-y)$$

An exactly homogeneous record must be infinitely long so that there are no end effects. But the eigenfunctions on an infinite domain are no longer enumerable and the eigenvalues become continuous functions, i.e., $\lambda_k$ becomes $\lambda(\omega)$.

Now, let $\phi_k(x)$ become $\phi(x,\omega) = e^{i\omega x}$ and divide both sides of Eq. (5) by $e^{i\omega y}$. Then Eq. (5) becomes

$$\int_{-\infty}^{\infty} K(x-y) e^{i\omega(x-y)} dx = \lambda(\omega) \qquad (13)$$

We see that the eigenfunctions of an infinitely long, homogeneous record are Fourier modes and the "eigenvalues" are the Fourier transform of the covariance matrix.

Stacking Variables

An interesting property of the ensemble functions $f_n(x)$ is that they do not have to be only one physical quantity. One can form a function $f_n(x_j)$ by stacking variables in it; e.g., for 2 variables

$$f_n(x_j) = \begin{cases} g(x_j), & j = 1, 2, \ldots, N \\ h(x_{j-N}), & j = N+1, N+2, \ldots, 2N \end{cases}$$

By doing so the covariance matrix $K(x_j, x_\ell)$ contains cross terms $E\{g(x_j)h(x_\ell)\}$. Here, g and h must have the same units since the eigenvalues have units of $f_n^2$. If they do not have the same units they either must be non-dimensionalized by their standard deviation, or some physically reasonable way of converting units of one variable in units of the other one must be found.

Theoretically there is no limit on the number of variables one may stack.

3. Eigenvectors of Homogeneous Correlation Matrices

a) As already mentioned in Section 2, if a process is homogeneous or stationary the autocovariance function $K(x,y)$ depends only on the separation distance $s = (x-y)$: $K(x,y) = K(x-y) = K(s)$. If $K(x,y)$ is represented by a discrete matrix $K_{ij}$, homogeneity means that the elements in a diagonal are equal. Such a matrix is called persymmetric. If $K(s)$ is normalized by the variance $K(0)$ it is called the autocorrelation function $R(s)$

$$R(s) = \frac{K(s)}{K(0)}$$

To test the effects of a finite domain on a homogeneous covariance function, the eigenfunctions for

$$R_1(s) = e^{-s/L}$$

were calculated. The integral scale is

$$\int_0^\infty R_1(s)ds = L$$

The calculations were made for a 9 x 9 matrix $R_{ij}$ where

$$R_{ij} = e^{-|i-j|\Delta x/L}$$

The maximum lag was always $\max|i-j| \cdot \Delta x = 1$. The resolution was $\Delta x = 0.125$. Since, $R(s)$ is a very smooth function, this resolution is high enough to pick up all the important features of $R(s)$.

A few tests were done with different resolutions but for the same maximum lag. Fig. 1 shows that the first eigenvector does not change much with changes in resolution.

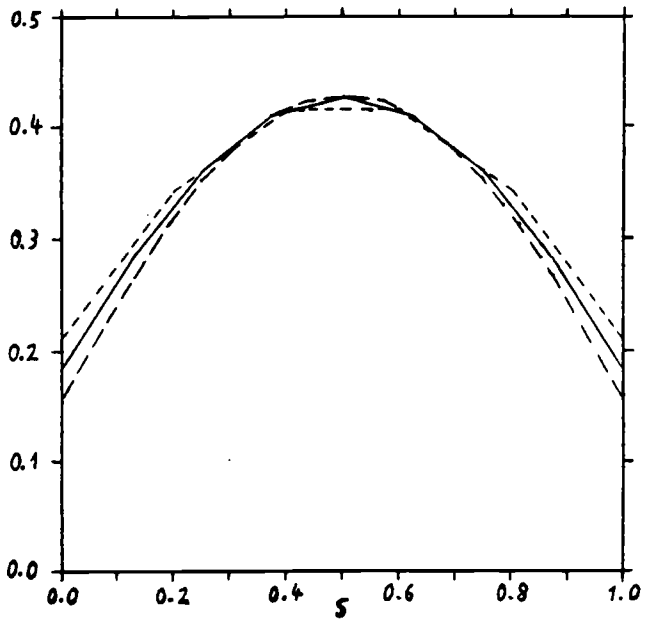


Fig.1: First eigenvectors of $R_1(s) = \exp|-8s|$ for different resolutions $\Delta x$: $\Delta x = 0.125$ (———), $\Delta x = 0.0625$ (— — —), $\Delta x = 0.2$ (– – – –).

**Table 1. Variance explained for different integral scales.**

| L | Variance explained (%) EV1 | EV2 |
|---|---|---|
| 1 | 71.76 | 15.13 |
| 1/2 | 54.91 | 20.87 |
| 1/4 | 36.74 | 22.48 |
| 1/8 | 22.41 | 18.59 |

$$R(s) = e^{-|s|/L}$$

In Fig. 2 the 1st and 2nd eigenvectors (EVs) are plotted for L = 1, 1/2, 1/4, 1/8. As the integral scale L decreases the 1st EVs become more and more like half a sine curve. This was to be expected since it corresponds exactly to increasing the maximum lag and in Section 2 it was shown that the eigenfunctions of an infinitely long, homogeneous record are Fourier modes. Also, it is interesting to note that the variance explained (VE) by the 1st EVs drops as L decreases (Table 1). This occurs because the components of the 1st EVs are fairly constant but R(s) decreases more rapidly for smaller L.

The eigenvectors of two other functions were calculated. They are:

$$R_2(s) = e^{-(\pi/4)(s/L)^2}, \quad \text{with integral scale L}$$

$$R_3(s) = (1 - \frac{s}{L})e^{-s/L}, \quad \text{with integral scale 0}$$

$R_2(s)$ has negative curvature at s = 0 and $R_3(s)$ crosses zero at s = L. Their eigenvectors are plotted in Fig. 3 for L = 1/2.

As can be seen the EVs of $R_1$ and $R_2$ are very similar. Also, the variance explained by EV1 and EV2 is higher for $R_2$ then for $R_1$ because $R_2(s) \geq R_1(s)$ for small s.

$R_3(s)$ looks most similar to the autocorrelation function of geophysical turbulence. The variance explained by EVs 1 and 2 is almost equal. In fact, $R_3(s)$ has a minimum value at s = 2L and for L < 1/2 this minimum is inside the limits of the matrix. Then EV1 has a form like EV2 for L > 1/2 and vice versa. Still, the eigenvectors look almost like Fourier modes.

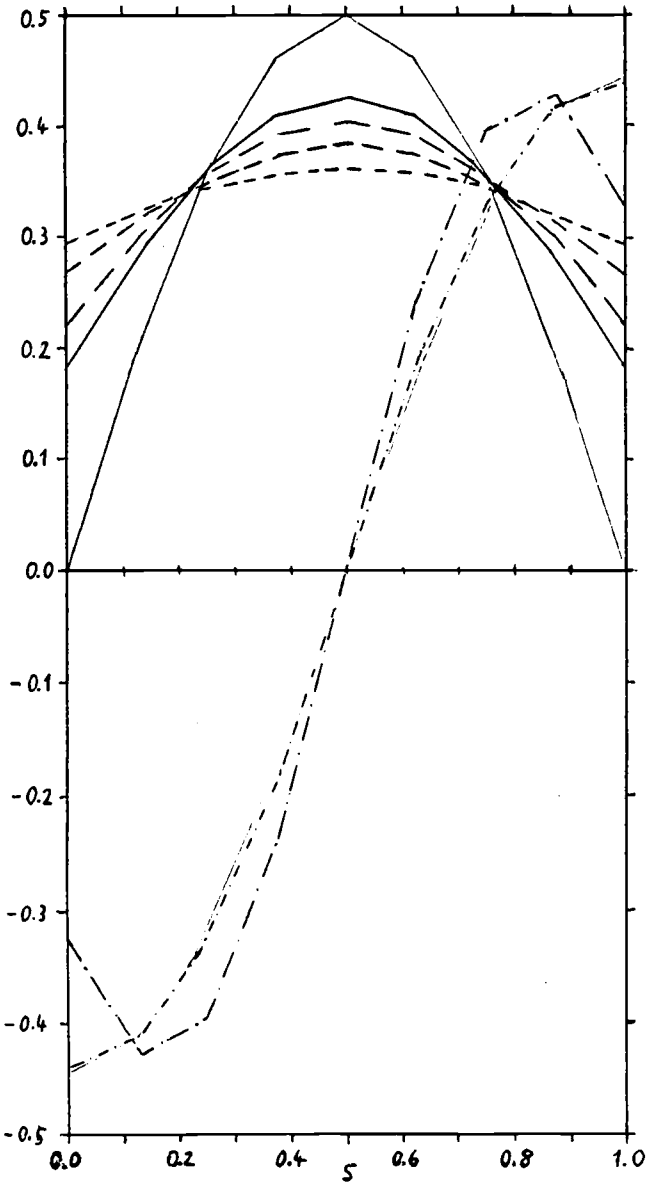


Fig.2: First eigenvectors of $R_1(s) = \exp|-s/L|$ for L = 1/8 (———), L = 1/4 (— —), L = 1/2 (— — —), L = 1 (— — — —). Second eigenvectors for L = 1/8 (—·—·), and L = 1 (—··—··). The thin curves are half a sine- and a cosine-function with the same resolution as the eigenvectors and normalized to length 1.

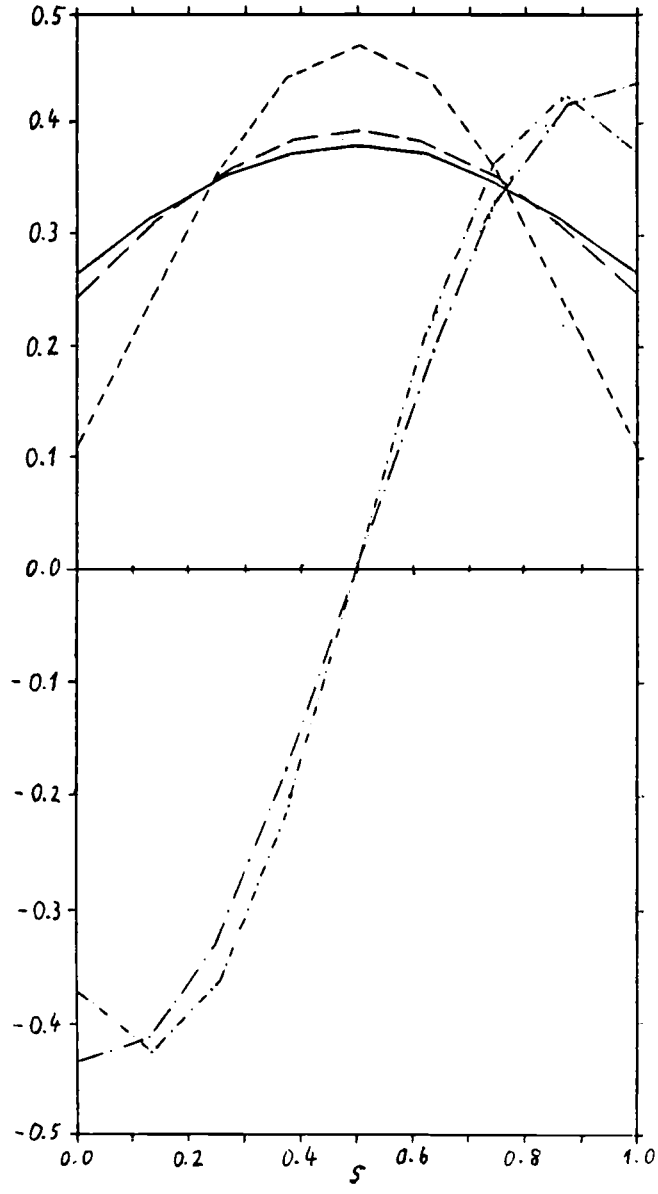


Fig.3: First eigenvectors of $R_1(s)$ (———), $R_2(s)$ (— — -), and $R_3(s)$ (– – – –). Second eigenvectors of $R_2(s)$ (— · — ·) and $R_3(s)$ (– · – · –) L = 1/2 for all correlation functions.

b) Other calculations were made simulating the correlation matrix of an observation vector of two stacked variables. Here the matrix looks like

$$R = \begin{bmatrix} R_{11} & R_{12}^T \\ R_{12} & R_{22} \end{bmatrix}$$

where $R_{11}$ and $R_{22}$ are autocorrelation matrices and $R_{12}$ is a crosscorrelation matrix. Results are shown where

$$R_{11} = R_{22} = e^{-|s|/L}$$

$$R_{12} = b \cdot \left(1 - \frac{|s+0.25|}{2L}\right) e^{-\frac{|s+0.25|}{L}} \qquad L = 1/2$$

b determines the maximum value of the crosscorrelation which occurs at s = -0.25 (i.e., off the main diagonal).

Fig. 4 shows the 1st EV for b = 0.1 and b = 0.8. The components of each of the two stacked variables versus the lag s are plotted. They look quite similar. This is confirmed by the measure of similarity of Section 2, i.e., the square of the scalar product of the vectors. Table 2 shows $\rho^2 = [\vec{e}_1(b = 0.01) \cdot \vec{e}_1(b)]^2$ ($\vec{e}_1$ = EV1) for different values of b. For all calculated values of b it is bigger than 0.9848 which corresponds to angles of less than 0.124 rad = 7.08°.

The shift of s = -0.25 where the maximum of the crosscorrelation $R_{12}$ occurs is visible in the maximum of the eigenvectors only for b > 0.1; it is 0.25. For b $\leq$ 0.1 it only makes the components of one

Table 2. Similarity between the first eigenvectors of matrices with different maximum cross correlation.

$$R_{12}(s) = b \cdot \left(1 - \frac{|s+0.25|}{2L}\right) e^{-\frac{|s+0.25|}{L}}, \qquad L = 1/2$$

$$\rho^2 = [\vec{e}_1(b=0.01) \cdot \vec{e}_1(b)]^2$$

| b | $\rho^2$ | $\alpha$ = arc cos$\rho$ (°) |
|---|---|---|
| 0.01 | 1.0000 | 0.00 |
| 0.10 | 0.9996 | 1.15 |
| 0.20 | 0.9977 | 2.75 |
| 0.40 | 0.9932 | 4.73 |
| 0.60 | 0.9887 | 6.10 |
| 0.80 | 0.9848 | 7.08 |

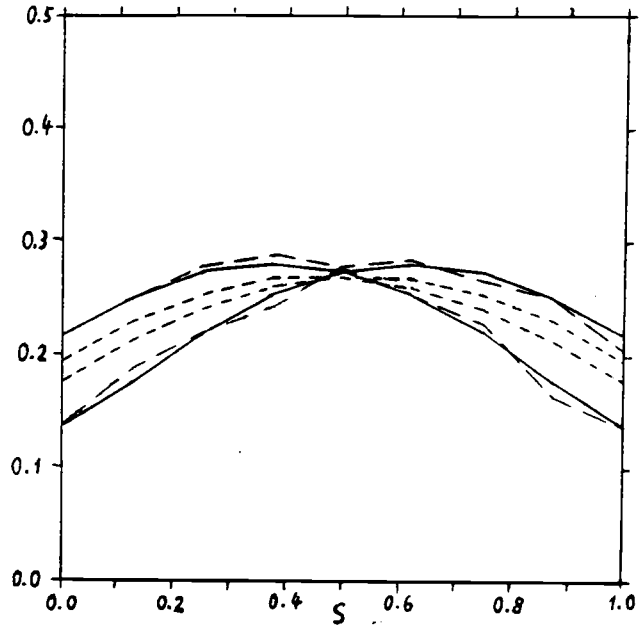


Fig.4: First eigenvectors of a correlation matrix R(s) of two stacked variables for different amplitudes b of the maximum crosscorrelation. (See text for the functional form of R(s).) b = 0.1 (- - - -), b = 0.8 (———), b = 0.8 but white noise is added to R(s) (— — -). The two curves for each value of b represent the two variables.

**Table 3. Similarity between eigenvectors of an unperturbed and a perturbed correlation matrix and variances explained by them. Primed quantities are calculated from the perturbed matrix.**

| i | $(\vec{e}_i \cdot \vec{e}'_i)^2$ | $\alpha(^\circ)$ | VE(%) | VE'(%) |
|---|---|---|---|---|
| 1 | 0.9992 | 1.56 | 41.99 | 40.79 |
| 2 | 0.9978 | 2.69 | 19.49 | 18.29 |
| 3 | 0.9492 | 13.0 | 10.31 | 9.74 |

variable asymmetric relative to s = 0.5. If there is no shift in the maximum of $R_{12}$, the components of one variable are symmetrical for all values of b.

One half of the vector is symmetric to the other one (i.e., one variable is symmetric to the other one), because the two autocorrelation matrices $R_{11}$ and $R_{22}$ are equal. If $R_{11} \neq R_{22}$ this will not happen (see below).

As in the case of a single autocorrelation matrix, the EVs look quite similar to Fourier modes. Hence, the stacking of the variables mainly gives information on the phase between different variables. This seems to be the main advantage of EV analysis of homogeneous records over Fourier analysis. From co- and quadrature spectra one obtains the phase relation between two variables. But it is not possible to get the phase relation between two variables considering the influence of three or more variables at the same time. With EV analysis there is principally no limit to how many variables may be stacked in a new observation vector: the phase relation between any two of the variables in the EV can then be studied.

Tests were done on the stability of the first few eigenvectors. White noise was added to the correlation matrix and the eigenvectors of this perturbed matrix were calculated. The standard deviation of the noise was 0.05, which is 5% of the maximum correlation. The first eigenvector for b = 0.8 is plotted in Fig. 4. It is very close to the first eigenvector of the unperturbed matrix. Since $R_{11} \neq R_{22}$ for the perturbed matrix, the vector is not exactly symmetric.

Table 3 shows the resemblance of the eigenvectors of the perturbed and unperturbed matrix and the variances explained by these vectors. The noise has high frequency; therefore, it has negligible influence on the first few vectors. Higher index eigenvectors explain smaller scale features, and are more susceptible to noise. But, since they do not explain a lot of the variance, we are not interested in them.

The tests show that the first eigenvectors are quite robust.

## 4. Analysis of Turbulence in the Bora

The data analysed in this study were measured by the Electra aircraft over the Yugoslavian coastal range in March 1982 during ALPEX. All three velocity components, and potential temperatures are analyzed. Velocities were measured with a Rosemount variable capacitance pitot static tube. Temperature was measured by a modified Rosemount platinum resistance thermometer. Potential temperature was obtained by multiplying by the static pressure (Kennedy, 1982; Wyngaard et al., 1978). For this study the horizontal u-velocity component is in the flight direction, which is southwestward. This is also approximately the direction of the "Bora", a strong, cold wind flowing over the coastal range and descending to the coast. The v-component is to the left of the u-component. The aircraft flew with a speed of 120 m/s plus or minus 10% and the measurements were sampled with a frequency of 20 Hz. So, they are approximately 6 m apart.

Where the Bora flows down the steep mountains to the coast, strong turbulence develops. This study attempts to find the structure of the main eddies with an eigenvector analysis of the (u,v,w,T)-correlation matrix where the correlations are evaluated for different lags, s. The maximum lag is 912 m. Inspection of the record showed that on the average, up- and downdrafts are typically 300 m wide. Thus, in one eigenvector, an up- or downdraft could be captured in the center, and roughly the same width in front and behind it. For the strongest turbulence, the velocity variances at these scales are approximately equal for all three components.

To save computation time, a resolution of only 48 m was used. Therefore, the eigenvectors contained 20 components for one quantity

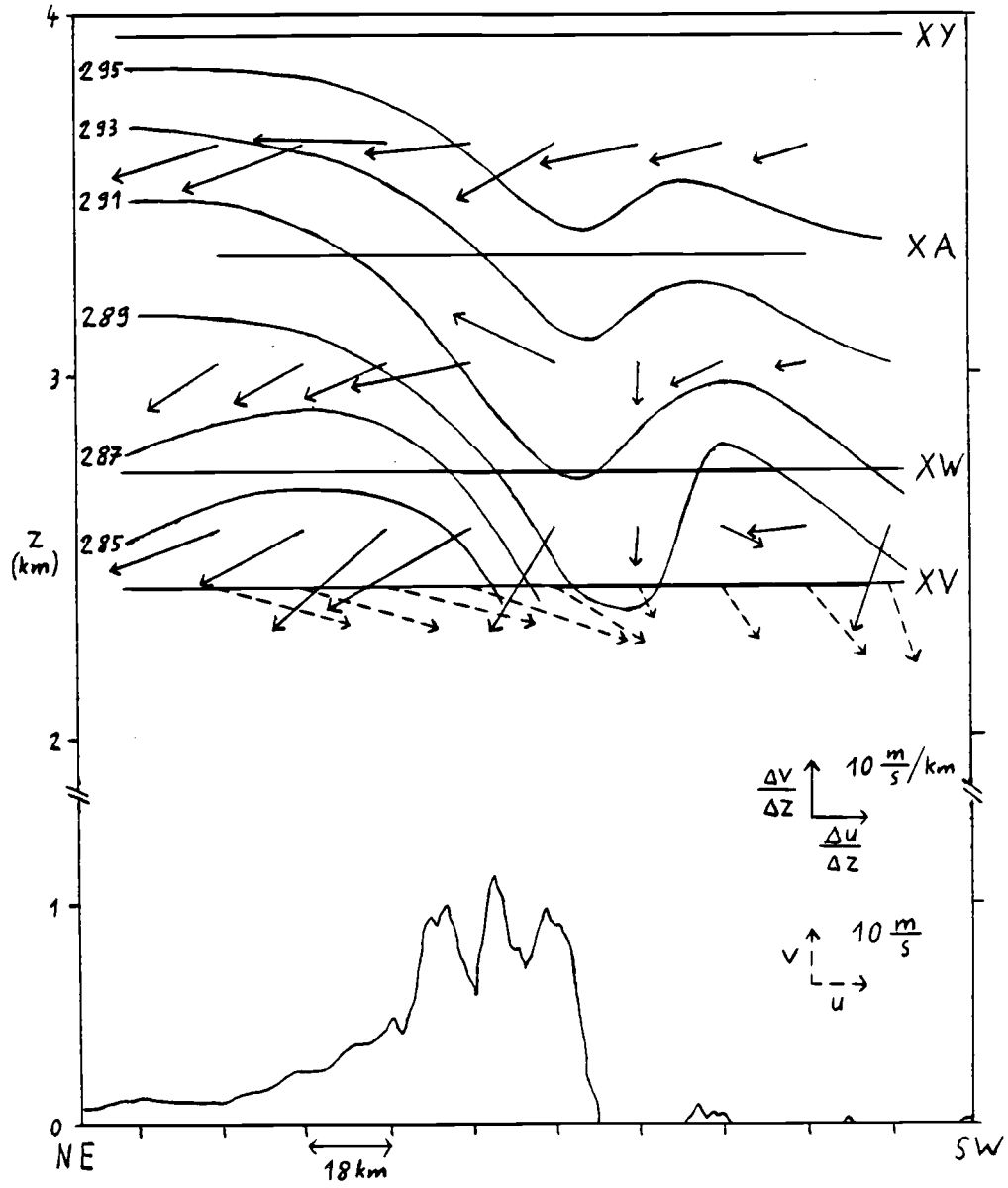


Fig.5: Block averaged wind shear vectors (solid arrows) and wind vectors for the lowest flight leg XV (dashed arrows). Straight lines are the flight legs XV to XY. Curved lines are isentrops of constant potential temperature θ. The surface profile is for leg XV. The cross section is from the northeast to the southwest.

and 80 components altogether. A few eigenvectors were calculated with higher resolution, but the resulting first few eigenvectors did not change significantly from 48 m resolution.

The records are almost homogeneous so that the autocorrelation matrices would be almost persymmetric if averaged over a whole record. Then the eigenvectors would be very similar to Fourier modes. To avoid this degeneracy, two alternative methods of calculating the correlation matrix were used.

The first one is normal conditional sampling, and it is described in Section a. The other method is called continuous weighting because weights can take any value between 0 and 1, as opposed to conditional sampling where a sample is either accepted with its full amplitude or rejected. Continuous weighting and its results are described in Section b.

a) Conditional sampling

This method was used to look for extrema in the gradient of the vertical velocity w. One of the characteristics of turbulence is a concentrated velocity gradient. When the velocities are Fourier transformed, then the sharp gradients spread energy over a very wide range in wavenumber space. Therefore, Fourier modes are not efficient to describe turbulence when gradients are the main quantities of interest. However, it might be possible to describe the sharp gradients with only very few eigenvectors.

We looked separately for maxima and minima of $\Delta w = w(s + 24\ m) - w(s - 24\ m)$. In this paper only results for minima will be presented. For maxima of $\Delta w$ the results are similar. If $|\Delta w|$ exceeded a

specified minimum value, a sample of 20 points (912 m) with the minimum of $\Delta w$ in the center was taken from the observations. To obtain more samples they were allowed to overlap half of their length. Consequently, not all samples are completely independent of each other.

Since gravity waves and trends have negligible influence on the gradient at the 48 m scale, raw unfiltered data could be used. To prevent the correlations from being dominated by the correlations of the different means of the samples, each sample was demeaned separately before the correlations were calculated.

Figures 6 and 7 show the first and second eigenvectors for samples selected with the criterion $\Delta w \leq -2.416$ m/s. (2.416 m/s is twice the standard deviation of $\Delta w$ for a combination of parts of leg XV, XW, and XA. By combining several legs, more than 80 samples were obtained. For comparison, the same limit was kept for the individual legs. For $\Delta w \geq 2.416$ m/s the correlations for the combined legs were dominated by one sample taken where two legs joined. This has no physical meaning and makes comparisons impossible.) They show vectorplots of the velocity vectors at every other leg. Solid arrows lie in the x-z-plane, and dashed arrows point in the y-direction. Solid arrow tips mean cold temperature perturbations and open tips mean warm temperature perturbations. Since the orientation of an eigenvector can be either way, the vectorplots were made such that $\Delta w < 0$ in the center of the eigenvector. With this orientation, the means of the expansion coefficients of the eigenvectors are positive, as would be expected. (Plots of the three velocity components and potential temperatures are in the appendix.)

Figures 6a and b show eigenvectors from samples of flight leg XV, and Figures 7a and b are for leg XW. Forty samples were collected from leg XV, and 39 samples from leg XW. This means that there are only 40, or 39, non-zero eigenvalues, and only 39, or 38, independent eigenvectors. This does not seem crucial if only the first two eigenvectors are considered, but high index eigenvectors are not significant.

The region from which the samples were taken are indicated in Figure 5. It shows the mean horizontal velocity shear vectors calculated by block averaging over 150 s, or 3000 observations. Upstream of the coast the bulk shear is mainly in the u-velocity component, $\partial u/\partial z < 0$, opposite to the flight direction. Downstream of the coast it is mainly in the v-component, $\partial v/\partial z < 0$. Over the coast, in the region of strongest turbulence, the shear becomes noisy. Local variations of the shear are larger than the average shear. Figure 5 also shows the block averaged horizontal velocity vectors for leg XV, and isentropes of constant potential temperature, $\theta$.

For leg XV, the first eigenvector (Figure 6a) shows upward motion of cold air on one side of the vector, and downward motion of warm air on the other side. This means that the vertical heat flux is down the mean temperature gradient (gradient transfer). The u-component is small except near the center. If we try to superimpose a plausible eddy structure on the velocity vectors, its axis of rotation would lie roughly between the y- and z-axis as drawn in Figure 8a. This picture is very tentative. It assumes that the eddy rotates like a cylinder and that the aircraft flew through the center of the eddy. The second assumption is justified if we assume that the aircraft randomly

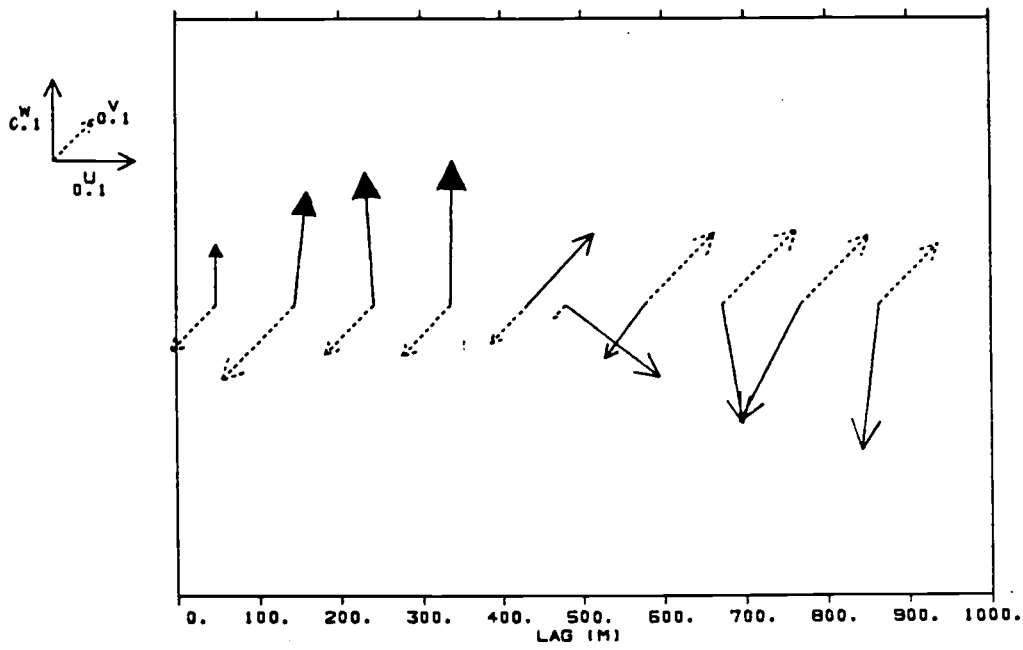


(a)

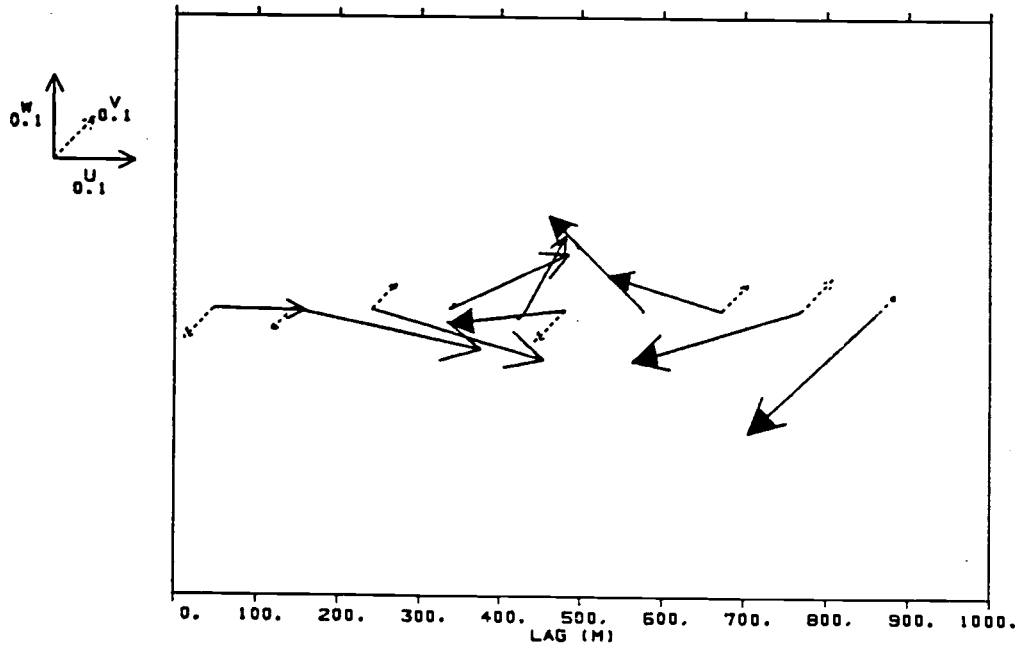


(b)

Fig.6: Eigenvectors for conditional sampling for leg XV: a) first eigenvector, variance explained (VE) = 17.0 %, b) second eigenvector, VE = 11.1 %. Solid arrow tips mean cold air, open tips mean warm air. Flight direction is southwestward.

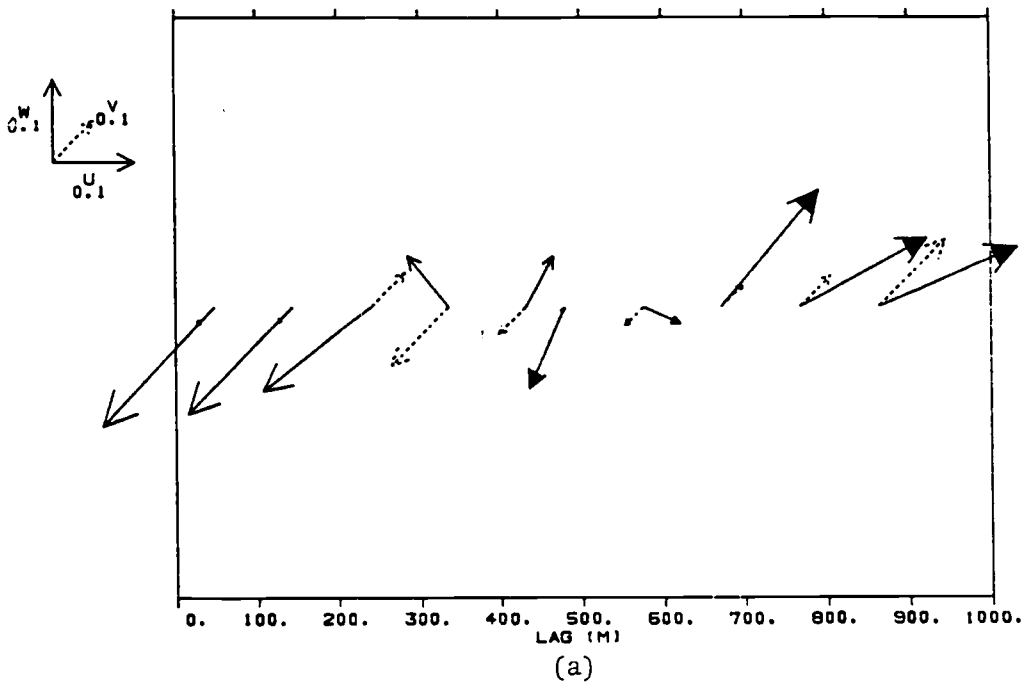


(a)

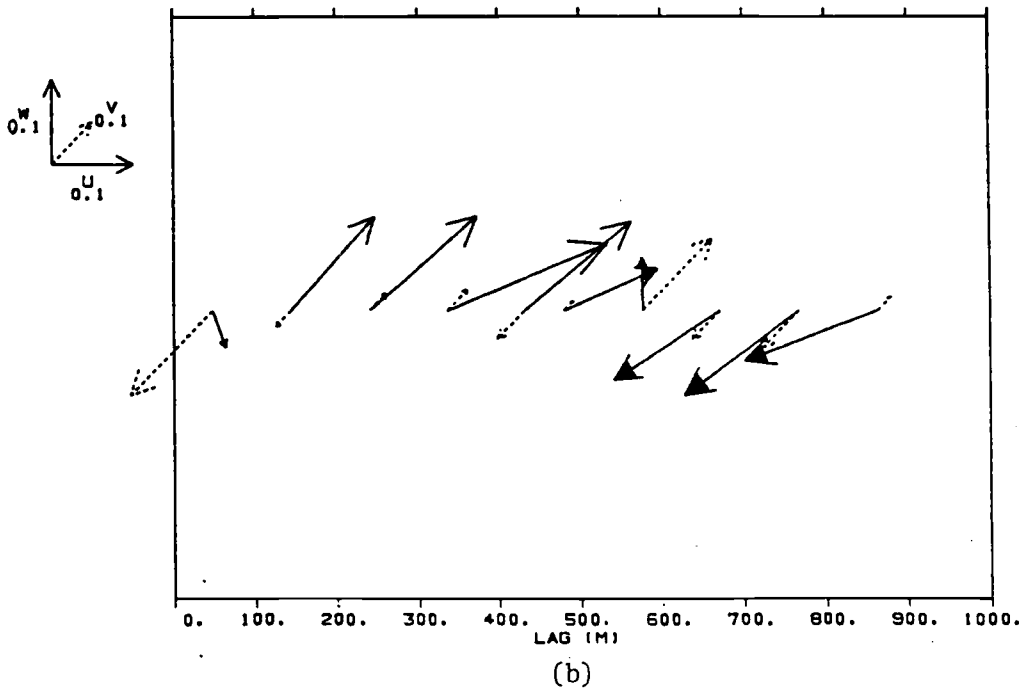


(b)

Fig.7: Eigenvectors for conditional sampling for leg XW: a) first eigenvector, VE = 19.4 %, b) second eigenvector, VE = 11.6 %. Solid arrow tips mean cold air, open tips mean warm air. Flight direction is southwestward.

intersected the eddies. Then, the velocities of intersections through the top and through the bottom of the eddies cancel each other. Also, with this data which is measured along one line, it is not possible to detect pure rotations with an axis in the flight path, since, for such rotation all three velocity components are independent of x and would be removed as trend.

The vertical flux of momentum orthogonal to the flight direction, wv, is negative. This would be up the mean gradient of v (countergradient) if the bulk shear vectors of Figure 5 are correct; but it was already mentioned that this is doubtful. In addition, momentum could be transported by pressure fluctuations which were not measured. All samples include only approximately half the observations from the sampled region, and the total mean correlation $\overline{w(s)v(s)}$ averaged over all legs s and all samples is negative.

The second eigenvector (Figure 6b) shows convergent motion associated with rising air, or divergent and sinking motion if it had opposite orientation. The largest flux is the heat flux in flight direction, $u\theta > 0$. There is no uniform mean gradient of $\theta$ over the region from which the samples were taken. But we might conclude that the horizontal heat flux in the flight direction is concentrated in regions were the flow converges or diverges.

For leg XW the first eigenvector (Figure 7a) seems to show mainly shearing motion between rising cold air and sinking warm air. The vertical momentum fluxes are consistent with the bulk shear which is bigger and seems more trustworthy than for leg XV. In the center of this vector there is motion in the opposite direction. It seems that the large shear motion produces a counterrotating eddy. The heat

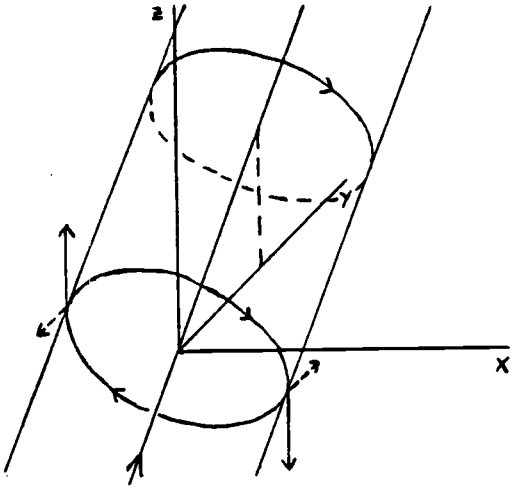


(a)

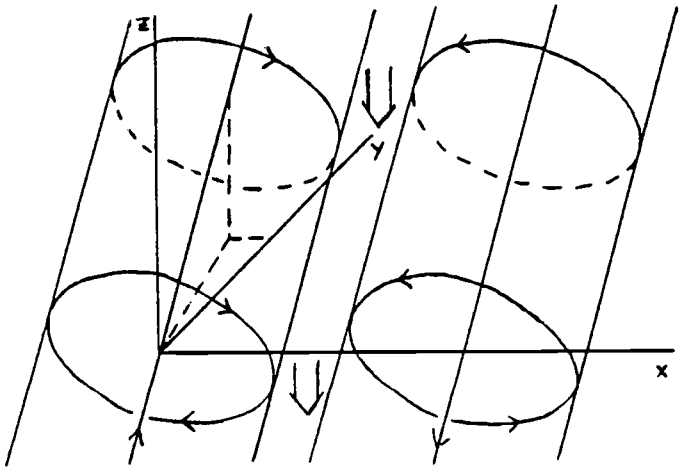


(b)

Fig.8: Eddies which might produce the velocity fields of the eigenvectors. a) Eddy corresponding to the velocity field of figure 6a. b) Downdraft produced by a double roller eddy.

fluxes are $w\theta < 0$ and $u\theta < 0$. $w\theta$ is gradient transfer, and $u\theta$ has the same sign as $\overline{u(s)\theta(s)}$ for all samples of this leg.

The second eigenvector (Figure 7b) shows similar shearing motion except that the heat flux is countergradient, and there is no counterrotating eddy in the center.

If we assume that the shearing motion comes from large ellipsoidal eddies, we can imagine, as Mahrt (1985), that the first eigenvector shows the first phase of turbulent overturning with cold rising, or warm sinking air. Then, the eddy starts disintegrating already and its air mixes a bit with the air of its environment. The second eigenvector represents this phase which is less clear, and therefore, the eigenvector explains less of the total variance of the flow.

Comparing the two legs, the vertical shear of the horizontal velocities, u and v, seem to be the main difference. On the upper leg, XW, the vertical shear of u exerts the main influence. For the lower leg, XV, the vertical shear is not well defined but in v it is stronger than for the upper leg. This influence of the different shear is clearly reflected by the eigenvectors.

b) Continuous weighting

Say we have a record of data from $x = 0$ to $x = L$, and we want the function which is most similar to the important events of the record. We can use (2), again, by replacing the expectation operator by the weighted integral over the whole record.

$$\lambda = \int_0^{L-\ell} g(x) \frac{\left[\int_0^{\ell} f(x+y)\phi(y)dy\right]^2}{\int_0^{\ell} \phi^2(y)dy} dx \qquad (14)$$

where $g(x)$ is the weighting function and $\ell$ is the expected width of the events. The weighting function determines which parts are considered important and which parts are unimportant.

The same calculations as in Chapter 2 lead to (5) again, but with a modified weighted covariance matrix. Now,

$$\tilde{K}(y,z) = \int_0^{L-\ell} g(x)f(x+y)f(x+z)dx \ , \qquad 0 \leq y, z \leq \ell. \qquad (15)$$

With this approach, we looked for extrema of w since the stronger updrafts and downdrafts are well-defined and lead to significant transport. Therefore, we took as the weighting function

$$g(x) = w^3(x+\ell/2) \ .$$

We sampled separately for up- and downdrafts. Advantages of this approach are that we do not have to prescribe conditions, like minimum allowed value for the magnitude of w, and an overlap criterion as with conditional sampling. We use all observations of the same sign, and not just part of the record.

This approach can lead to very few events dominating the whole record since we raise w to the third power. Also, if the extrema of w are broad, the edges of the up- or downdrafts as viewed by this method become diffuse. There are many other possibilities for weighting functions.

Because we use all observations, the calculations are expensive.

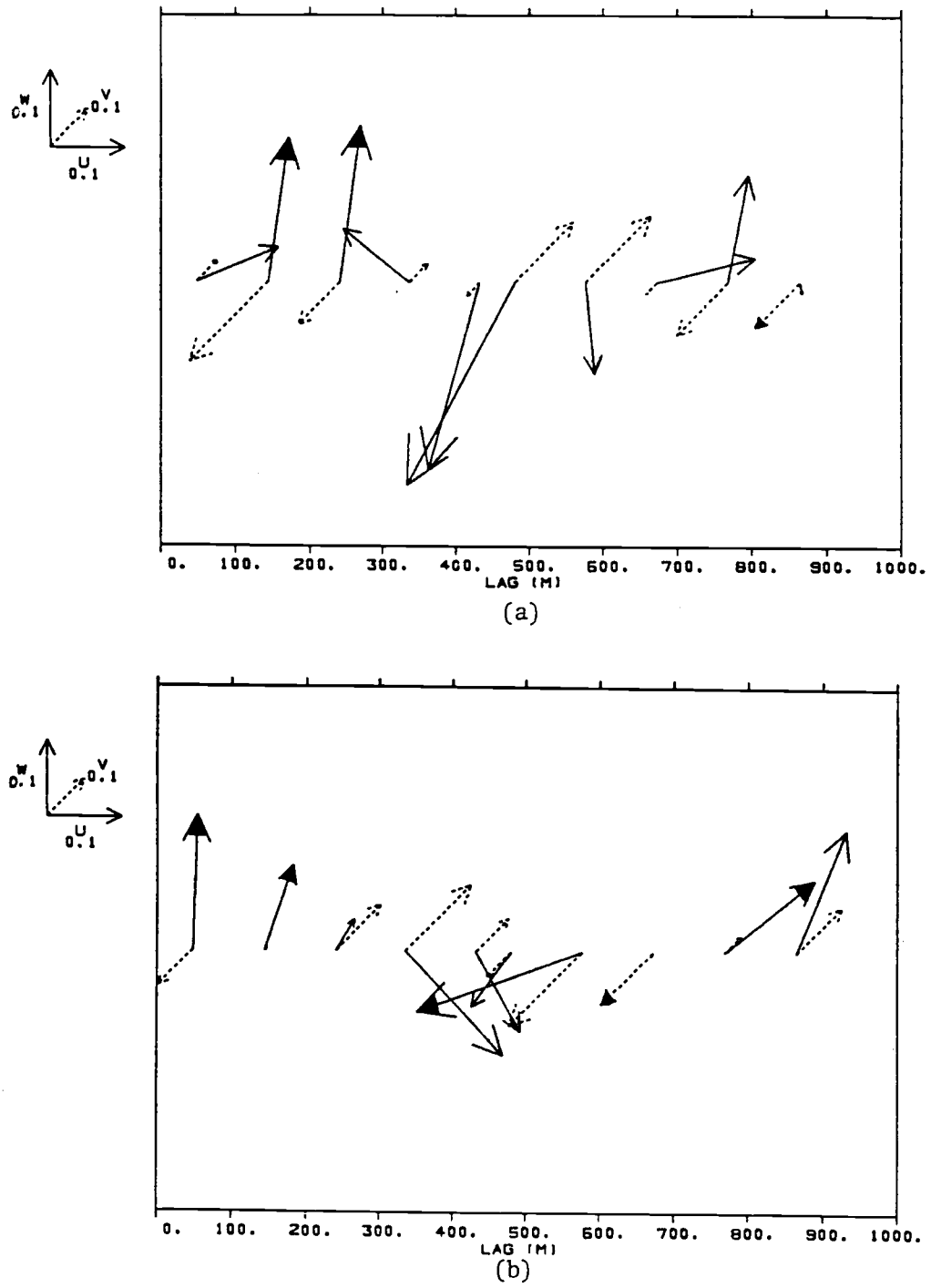


Fig.9: Eigenvectors for continuous weighting for leg XV: a) first eigenvector, VE = 11.4 %, b) second eigenvector, VE = 8.3 %. Solid arrow tips mean cold air, open tips mean warm air. Flight direction is southwestward.

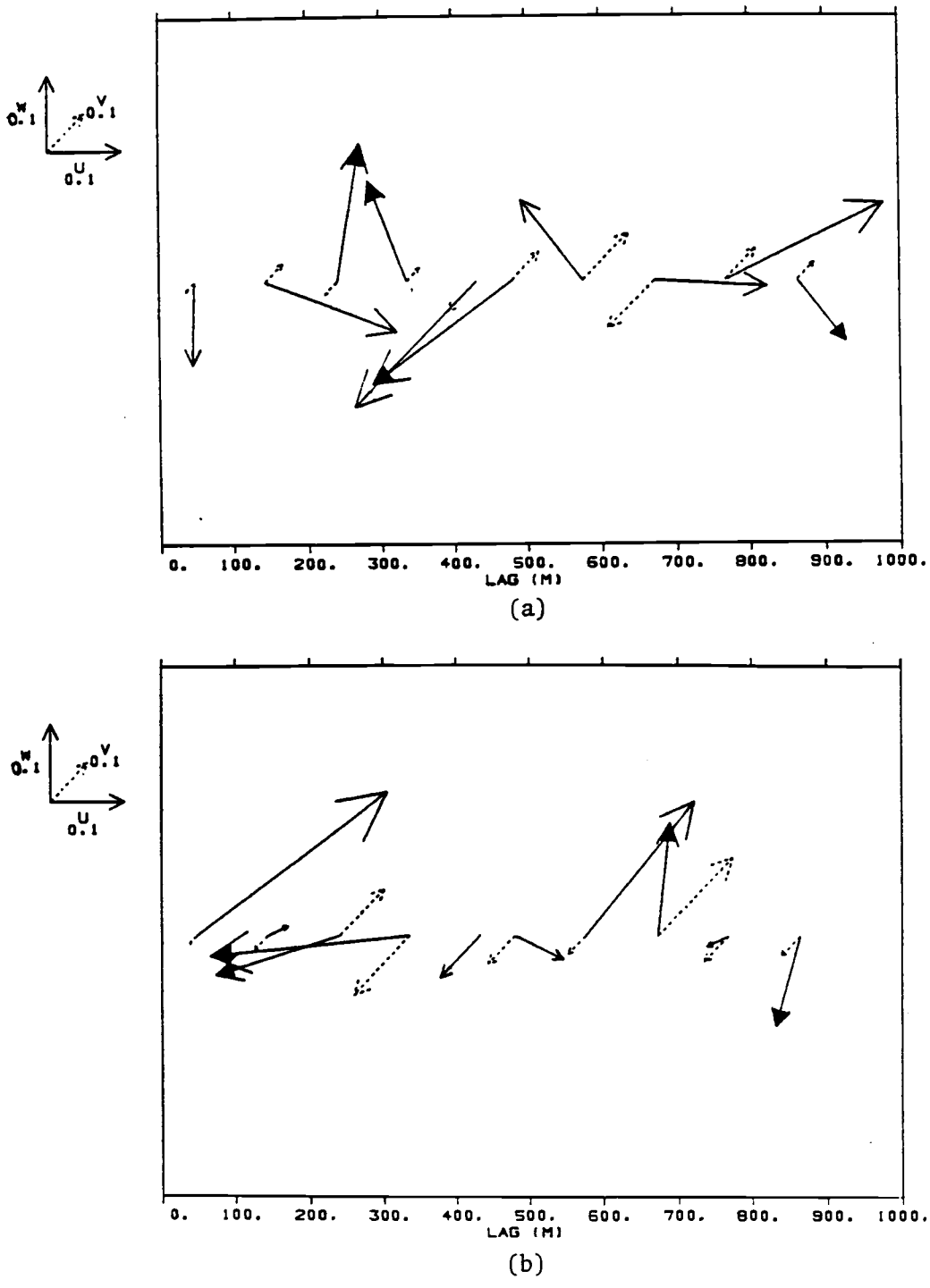


Fig.10: Eigenvectors for continuous weighting for leg XW: a) first eigenvector, VE = 25.1 %, b) second eigenvector, VE = 7.1 %. Solid arrow tips mean cold air, open tips mean warm air. Flight direction is southwestward.

Since we used this method to look for extrema of w, and not for extrema of small gradients, we cannot use raw data which contains wave motions and trends on a variety of larger scales. Instead, we used 1000 m high pass filtered data. Thus, the cut-off wavelength is a little bit longer than the maximum lag of the correlation matrices.

I shall compare the first two eigenvectors for a weighting function $w^3 < 0$, (i.e., for downdrafts), for leg XV and leg XW. Results for updrafts are not exactly the same, but similar. Figures 9a and b show the eigenvectors of leg XV, and Figures 10a and b those of leg XW. The first eigenvectors correspond to a downdraft in the center with updrafts on the sides. The vertical heat flux is downward which is gradient transfer. The downdrafts are tilted in the direction of the bulk shear in the u-component. For the upper leg, XW, the tilt is larger as is the shear. In general, the u-component seems much more important for leg XW than for leg XV. Also, the downdrafts seem narrower and weaker.

It is interesting to note that a double roller eddy, as drawn in Figure 8b, would fit the velocity vectors of the first eigenvector for leg XV quite well. But the axes of these eddies usually lean in the direction of the shear. Hence, the shear would have to be to the left of the flight direction. Then, $wv < 0$ could be explained with a mixing length model.

For the upper leg, XW, the double roller would be much narrower, but the arrows seem to be more random. However, this vector already explains 25% of the total variance. This might indicate that this leg is less turbulent, or that the correlations are more dominated by only a few events.

For leg XW, the second eigenvector shows up- and downdrafts in the shear direction. The downdraft has a pronounced peak. The vertical heat flux is upward which is countergradient. Perhaps it is again the second phase of overturning as explained in Section a.

The second eigenvector for leg XV looks more interesting. This could be a cut through a vortex with a vertical axis. The air seems to be drawn down as in the sink of a bathtub. Since we have only one-dimensional cuts through the flowfield it is quite possible that such a sink occurs more frequently but that we tend to draw eddies through the vectors if the pattern is not clear. The vertical heat flux is negative on the upstream side and mainly positive on the downstream side. Therefore, the net flux is small. The horizontal heat flux is $u\theta > 0$. This eigenvector looks similar to the second eigenvector for conditional sampling for leg XV (Figure 6b).

In comparing the different analyses we must keep in mind that they did not have the same selection criterion. One looked for minima of $\Delta w$, and the other one for minima of w. Still the eddies we get have similar axes of rotation. The eigenvectors of continuous weighting seem more noisy. At least part of this arises from using 1000 m high pass filtered data. Therefore, the motion has to be on scales less than 1000 m which looks more noisy.

## 5. Comparison with Boundary Layer Turbulence

The results of the eigenvectors of strong clear-air turbulence observed during ALPEX will be briefly compared with eigenvectors of turbulence data measured in the stable boundary layer. The measurements were taken during a fair-weather period in the "Severe Environmental Storms and Mesoscale Experiment" (SESAME) conducted in Oklahoma, in April and May of 1979. They were taken by aircraft early in the morning close to the ground. Due to radiative cooling this surface layer is very stably stratified.

The same analysis as with the ALPEX data was applied to the SESAME data. Since the aircraft flew with a speed of only approximately 80 m/s, the spatial resolution of the eigenvectors is only 32 m and the maximum lag is 608 m.

Figures 11a and b show the first and second eigenvectors for samples taken on 6 May. The sampling criterion was $\Delta w \leq -1.5$ m/s which is twice the standard deviation of $\Delta w$; 29 samples were obtained. On this day, the turbulence was relatively strong due to strong wind shear which was approximately 70° to the right of the flight directions. This shear is clearly shown by the first eigenvector. The stable stratification results in a downward heat flux. The second eigenvector mainly shows the same shearing motion. Only, the shear occurs at the sides of the eigenvector. All fluxes of the first and second eigenvector have the same sign as the total mean fluxes, and these are large. For the ALPEX cases the total mean fluxes were smaller. Clear-air turbulence seems to be more chaotic than boundary layer turbulence. In boundary layer turbulence, flow parameters scale with the distance from the ground which constrains

and organizes the motion.

Figures 12a and b show the first and second eigenvectors for samples taken on 5 May. The sampling criterion was $\Delta w \leq -0.22$ m/s which is again twice the standard deviation of $\Delta w$; 30 samples were available with this criterion. On this day, the stratification is very strong and the shear is weak; as a result, the turbulence is very weak. The first eigenvector shows shearing motion. This time it has approximately the same strength in the u- and v-components because the shear is approximately 45° to the left of the flight direction. The change from the upward to the downward motion is very abrupt. All four variables change sign almost exactly together. All vertical fluxes are gradient transfer. An eddy superimposed on the velocity vectors could be one of Townsend's (1976) double rollers since its axis of rotation would tilt roughly in the direction of the shear.

The second eigenvector could be the eddy which rotates in the opposite direction. Also, its axes of rotation would lie more in the y-z-plane. It seems to be smaller and the vertical heat flux is upward, which is countergradient. Probably, this is at least partly a consequence of the dominance of the first eigenvector. This vector explains already 27.1% of the total variance, and it gives a larger heat flux than is the total mean heat flux of all samples. The first and second eigenvectors together explain already 44.3% of the variance. This is a sign of not fully developed turbulence with only a few dominating types of motion. Also, the cascade of energy to smaller scale eddies is not developed. The first four eigenvectors of the samples taken on 6 May explain 43.2% of the variance. Also for

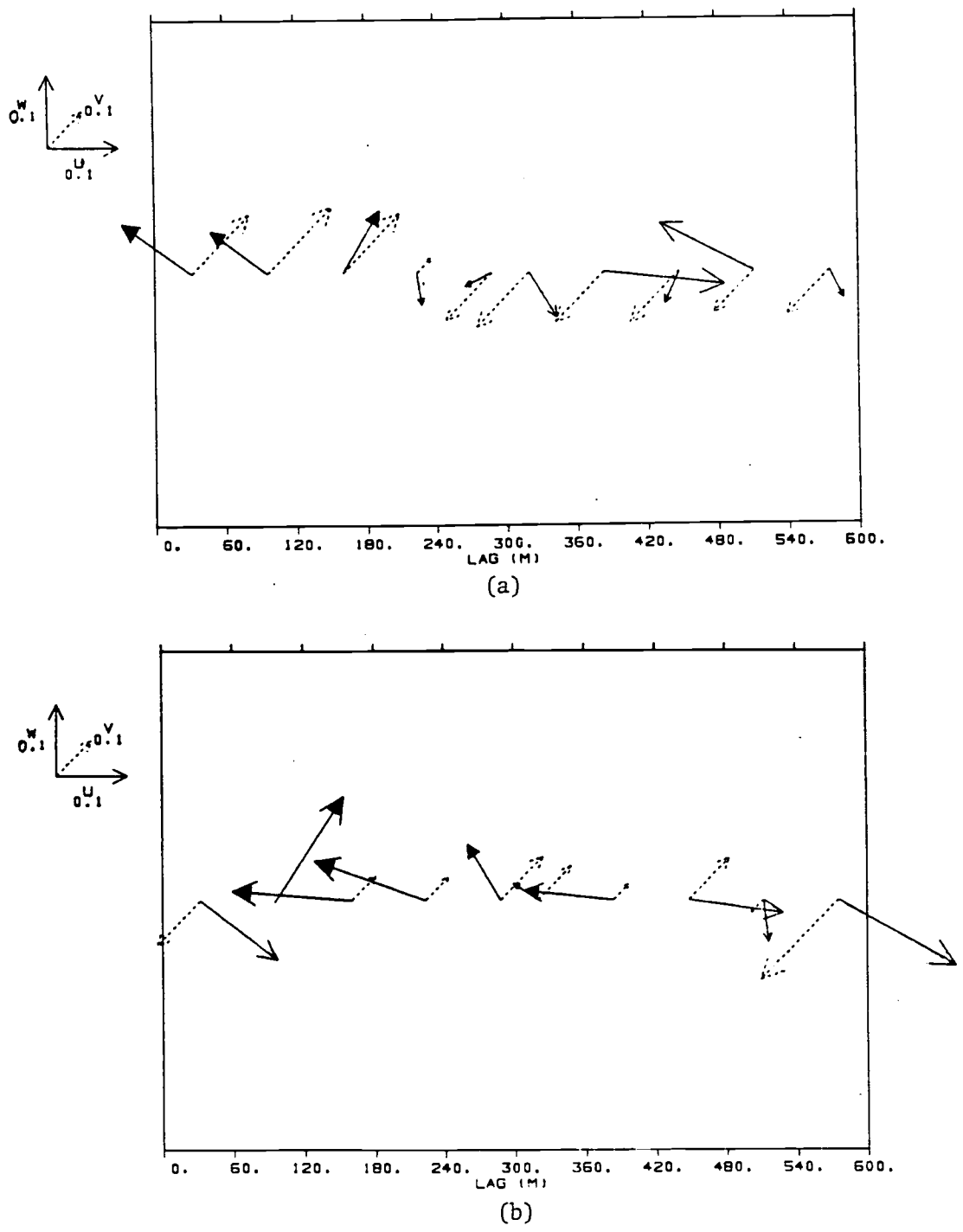


Fig.11: Eigenvectors for conditional sampling for SESAME, 6 May: a) first eigenvector, VE = 16.8 %, b) second eigenvector, VE = 10.2 %. Solid arrow tips mean cold air, open tips mean warm air. Flight direction is northward.

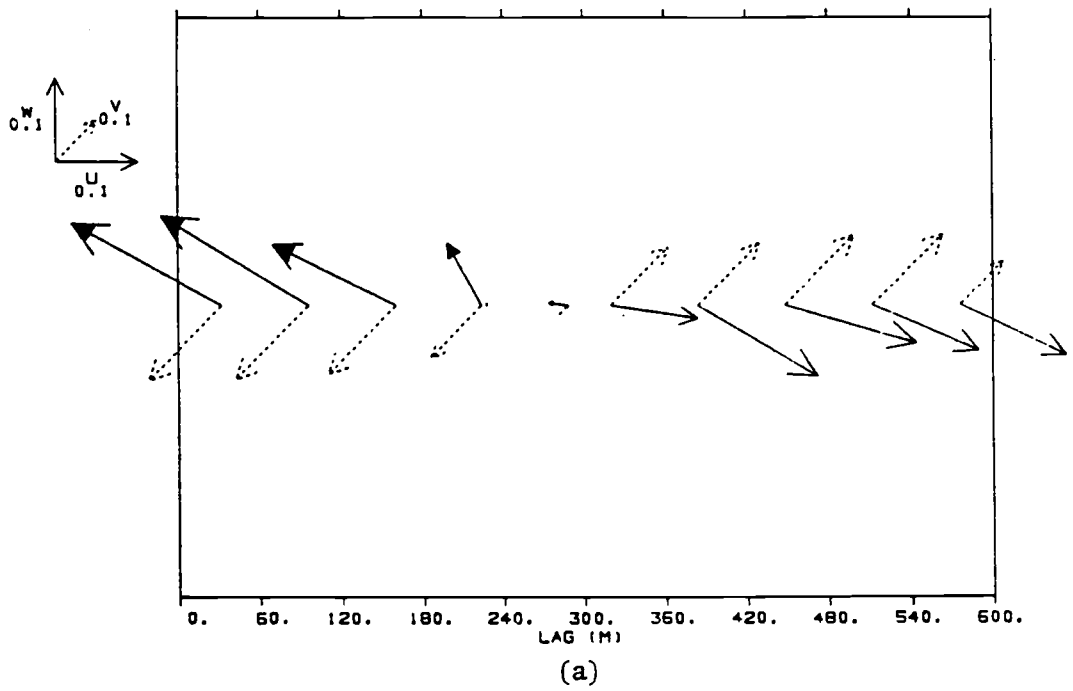


(a)

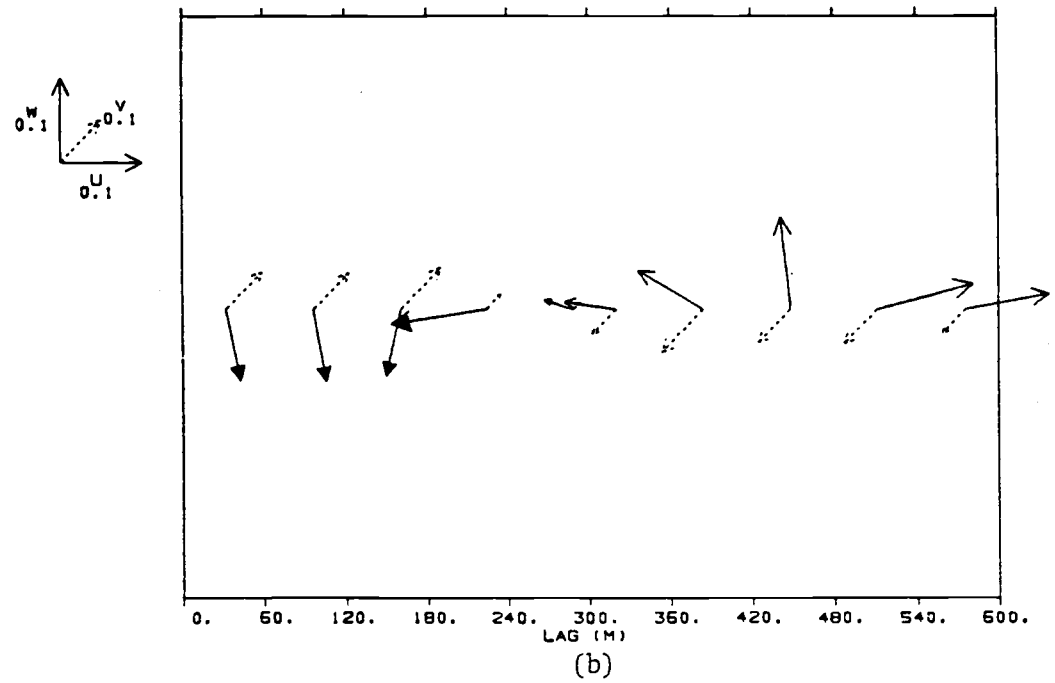


(b)

Fig.12: Eigenvectors for conditional sampling for SESAME, 5 May: a) first eigenvector, VE = 27.1 %, b) second eigenvector, VE = 17.3 %. Solid arrow tips mean cold air, open tips mean warm air. Flight direction is northward.

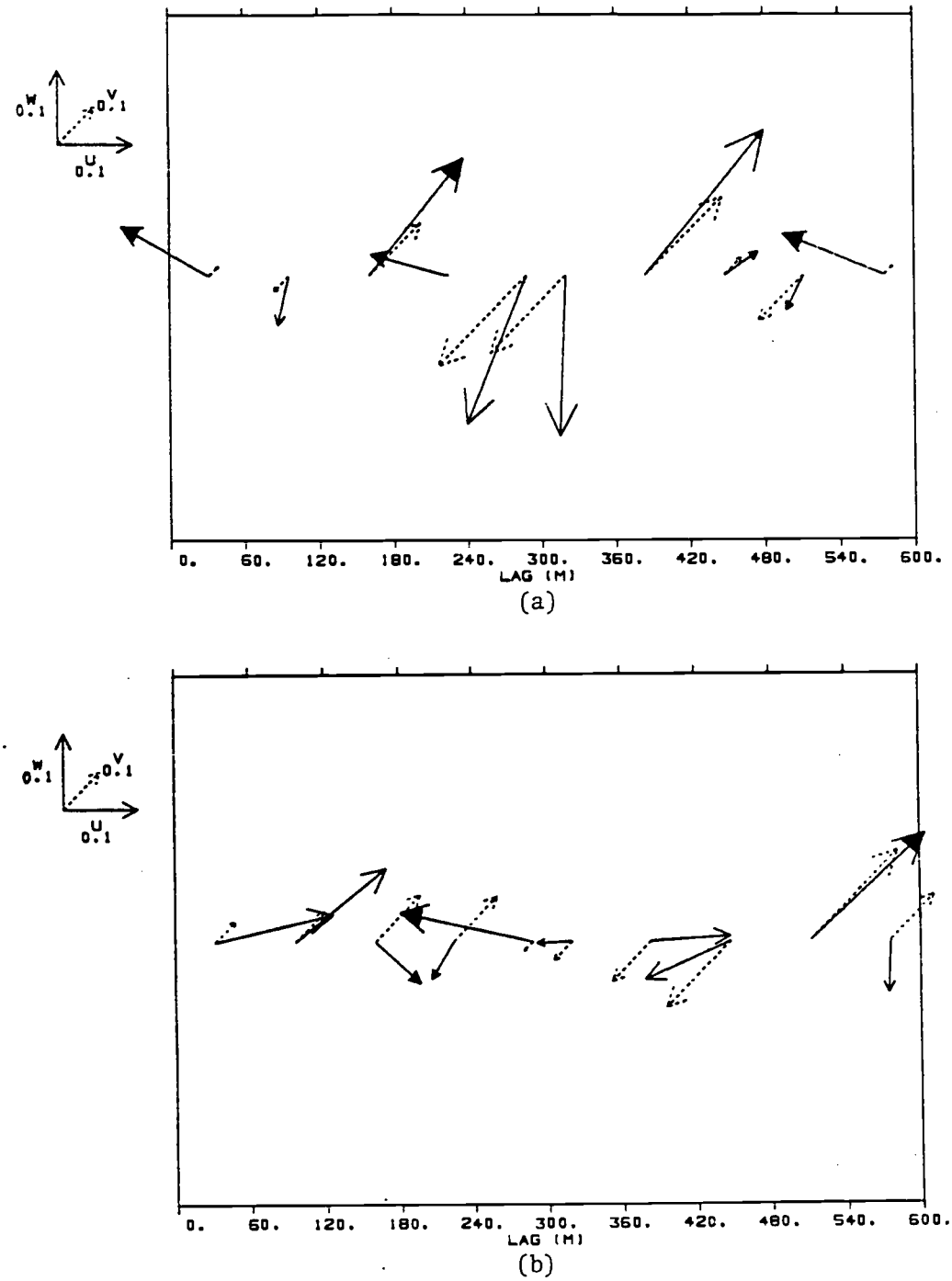


Fig.13: Eigenvectors for continuous weighting for SESAME, 6 May: a) first eigenvector, VE = 14.3 %, b) second eigenvector, VE = 9.3 %. Solid arrow tips mean cold air, open tips mean warm air. Flight direction is northward.

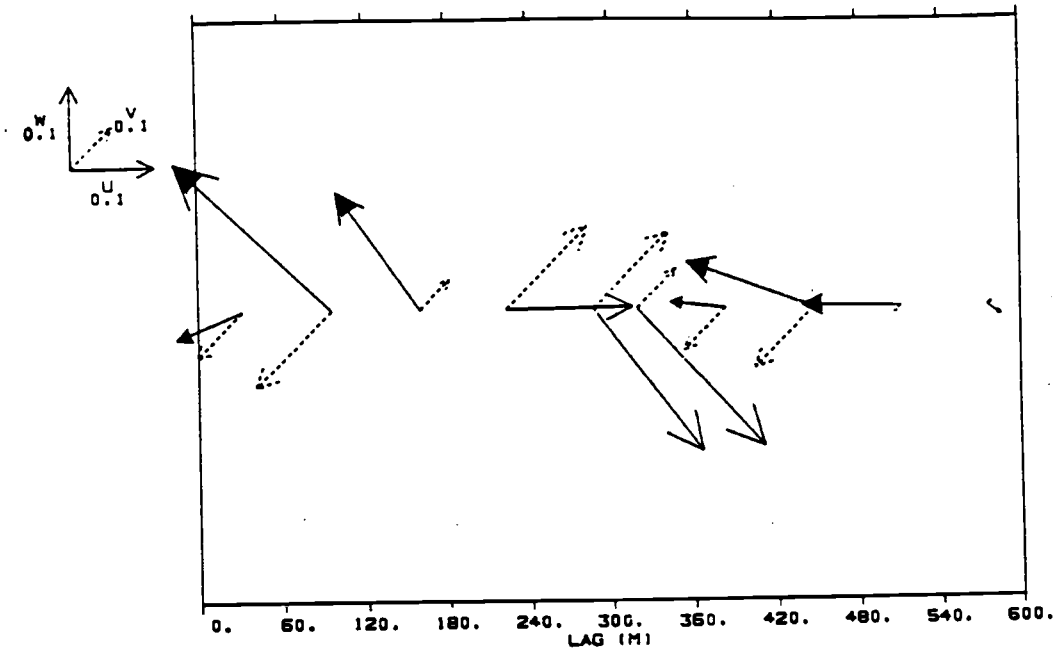


(a)

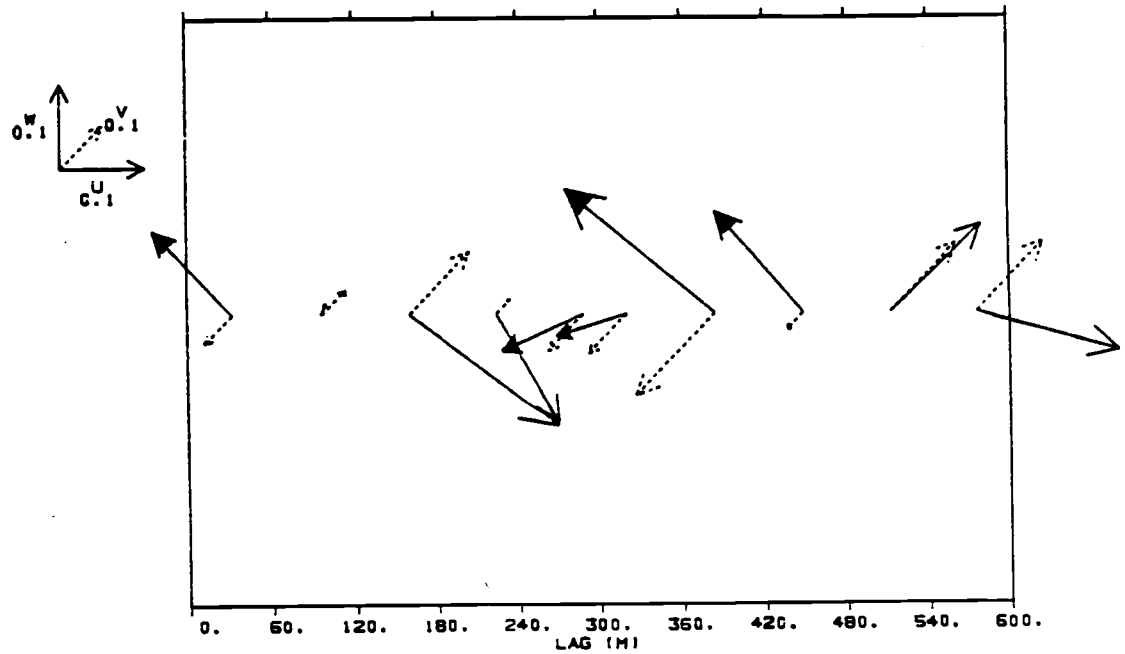


(b)

Fig.14: Eigenvectors for continuous weighting for SESAME, 5 May: a) first eigenvector, VE = 15.7%, b) second eigenvector, VE = 14.7%. Solid arrow tips mean cold air, open tips mean warm air. Flight direction is northward.

the ALPEX cases, four eigenvectors are needed to explain a similar amount of variance.

The eigenvectors of the correlation matrix for continuous weighting with $w^3 < 0$ agree very well with the eigenvectors for conditional sampling. Since the maximum lag is smaller than for the ALPEX data, 500 m high pass filtered data, instead of 1000 m high pass filtered data, was used in the analysis of the SESAME data.

Figure 13 shows the eigenvectors from 6 May and Figure 14 those from 5 May. The first eigenvector from 6 May shows a downdraft in the center. The gradient of w at the upstream side of this downdraft resembles very closely the gradient in the first eigenvector for conditional sampling. The second eigenvector shows no clear type of motion and in doing so it is similar to the second eigenvector for conditional sampling.

On 5 May, the first and second eigenvectors look very similar. In the second eigenvector, the maximum downdraft occurs a little bit upstream of the center. The velocity gradients upstream of the downdraft agree almost perfectly with those of the first eigenvector for conditional sampling on 5 May. This agreement is consistent with the idea of a double roller eddy whose axes of rotation lean in the direction of the mean shear approximately 45° to the left of the flight direction. Again, the first two eigenvectors from 5 May explain more variance than those from 6 May. The eigenvectors from 5 May explain 30.4% while those from 6 May explain 23.6% of the variance.

Comparing the eigenvectors of clear-air turbulence (ALPEX) with

those of boundary-layer turbulence (SESAME) the boundary-layer turbulence shows less variety of motion. Especially on 5 May, when the shear was weak and consequently the turbulence was very weak one type of motion, double roller eddies with axes of rotation tilted in the direction of the shear as proposed by Townsend (1976), appear to dominate the turbulence. This might be the initial stage of turbulence since, as already mentioned, a -5/3 region of the energy spectrum was not developed.

## 6. Conclusion

It was shown that it is possible to try to infer the structure of the main eddies of turbulence from data measured by aircraft. Two different methods of constructing the correlation matrix were shown. The eigenvectors of the correlation matrices resulting from the two different methods agree very well for boundary-layer turbulence which is less vigorous than clear-air turbulence. For clear-air turbulence the agreement between the methods is not as good, but this is at least partly due to a larger variety of motions. Also, it was not possible to estimate the small-scale variations of the mean shear direction in the most turbulent region of the bora.

In the case of weak turbulence in the very stable boundary layer Townsend's double roller eddy could be clearly identified. For strong turbulence, its axes of rotation did not tilt exactly in the shear direction and it was not so clearly defined.

## References

Busch, N. and E.L. Petersen, 1971: Analysis of non-stationary ensembles, in 'Statistical Methods and Instrumentation in Geophysics', ed. by A.G. Kielaas, Teknologisk Forlag, Oslo, 71-92.

Courant, R. and D. Hilbert, 1968: Methoden der Mathematischen Physik, Springer Verlag, pp. 469.

Dutton, J.A., 1969: A preliminary study of the probabilistic structure of turbulent forcing on launching vehicles, NASA - CR 1410.

Grant, H.L., 1958: The large eddies of turbulent motion. J. Fluid Mech., 4, 149-190.

Kennedy, P.J., (ed.), 1982: An ALPEX Aircraft Atlas, NCAR, Boulder.

Kutzbach, J.E., 1967: Empirical eigenvectors of sea level pressure, surface temperature, and precipitation complexes over North America. J. Appl. Meteor., 6, 791-802.

Lorenz, E.N., 1956: Empirical orthogonal functions and statistical weather prediction. Sci. Rep. No. 1, Contract AF19(604)1566, AFCRC-TN-57-256, AD 110268.

Lumley, J.L., 1965: The structure of inhomogeneous turbulent flows, in 'Atmospheric Turbulence and Radio Wave Propagation', ed. by A.M. Yaglom and V.T. Tatarsky, Nauka, Moscow, 166-176.

Mahrt, L., 1985: Vertical structure and turbulence in the very stable boundary layer. J. Atmos. Sci., 42, 2333-2349.

Payne, F.R. and J.L. Lumley, 1967: Large eddy structure of the turbulent wake behind a circular cylinder. Phys. Fluids (Supplement), 10, S194-S196.

Petersen, E.L., 1976: A model for the simulation of atmospheric turbulence. J. Appl. Meteor., 15, 571-587.

Townsend, A.A., 1976: The Structure of Turbulent Shear Flow, Cambridge University Press, 429 pp.

Wyngaard, J.C., W.T. Pennell, D.H. Lenschow, M.A. LeMone, 1978: The temperature-humidity covariance budget in the convective boundary layer. J. Atmos. Sci., 35, 47-58.

# Appendix

# Appendix

The appendix contains a different representation of the eigenvectors discussed in this study. In this representation it is possible to see the magnitude of the temperature perturbations. Figures A1-A8 correspond to Figures 6, 7, and 9-14 in the main part.

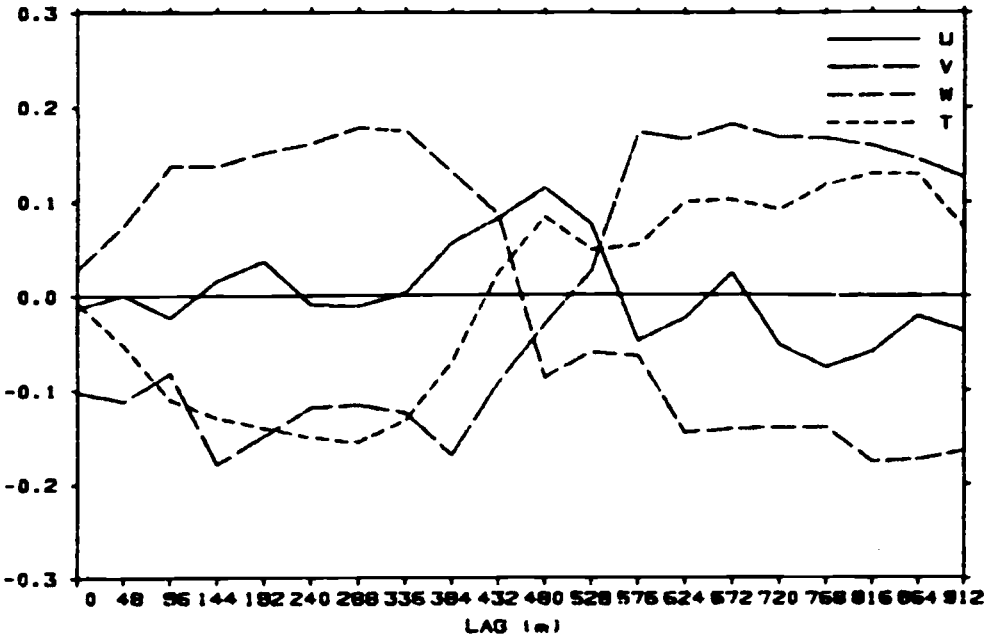


(a)

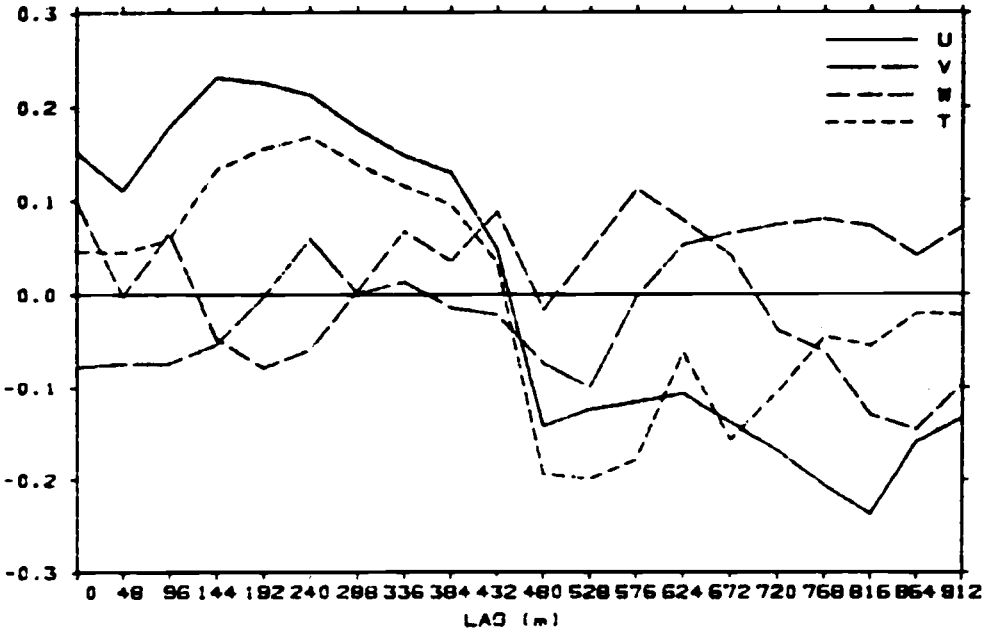


(b)

Fig.A1: First (a) and second (b) eigenvectors for conditional sampling for leg XV.

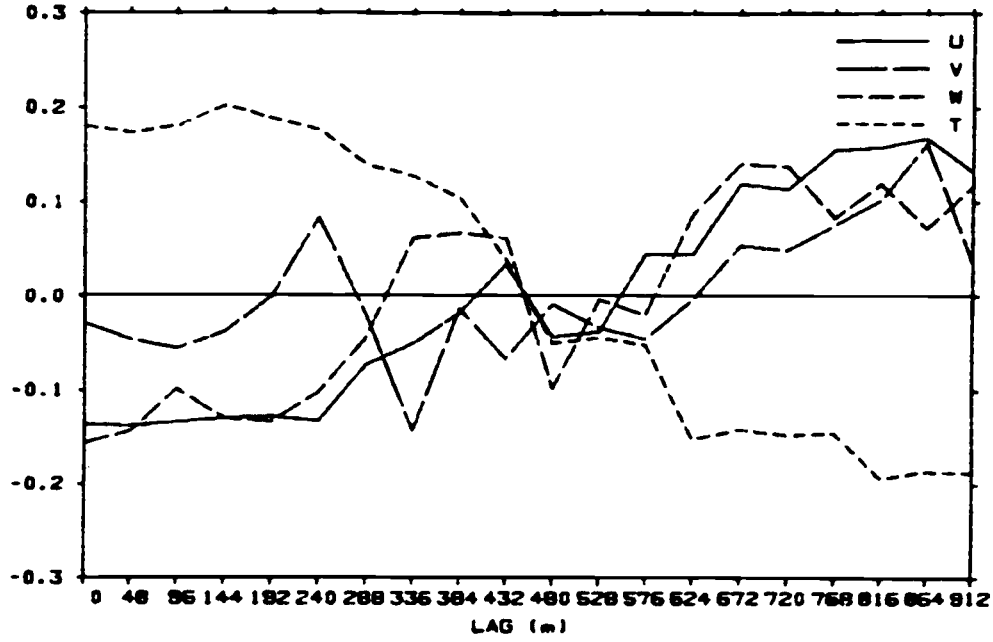


(a)

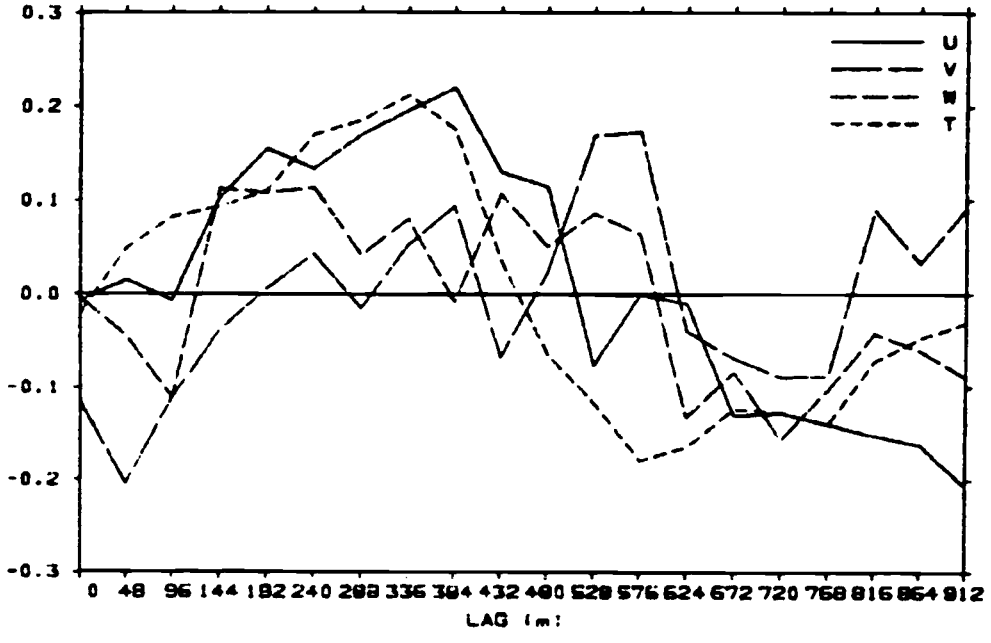


(b)

Fig.A2: First (a) and second (b) eigenvectors for conditional sampling for leg XW.

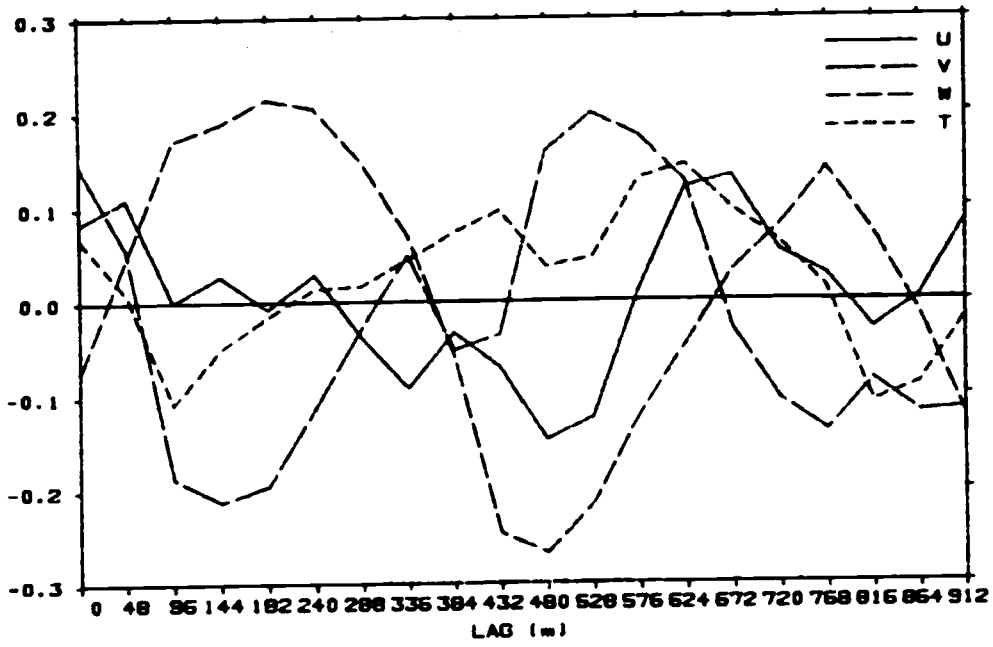


(a)

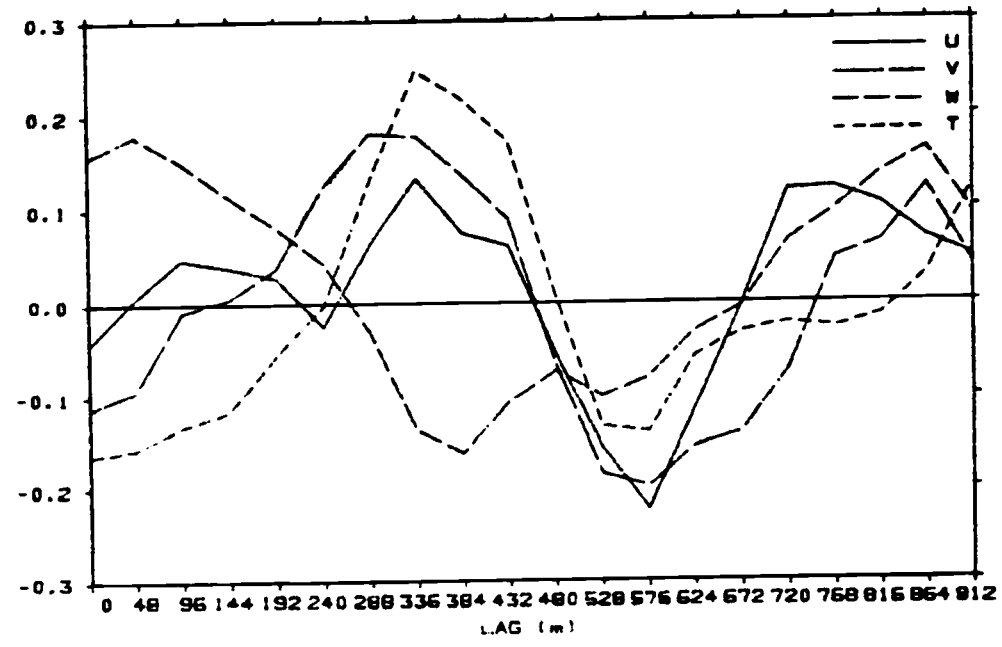


(b)

Fig.A3: First (a) and second (b) eigenvectors for continuous weighting for leg XV.

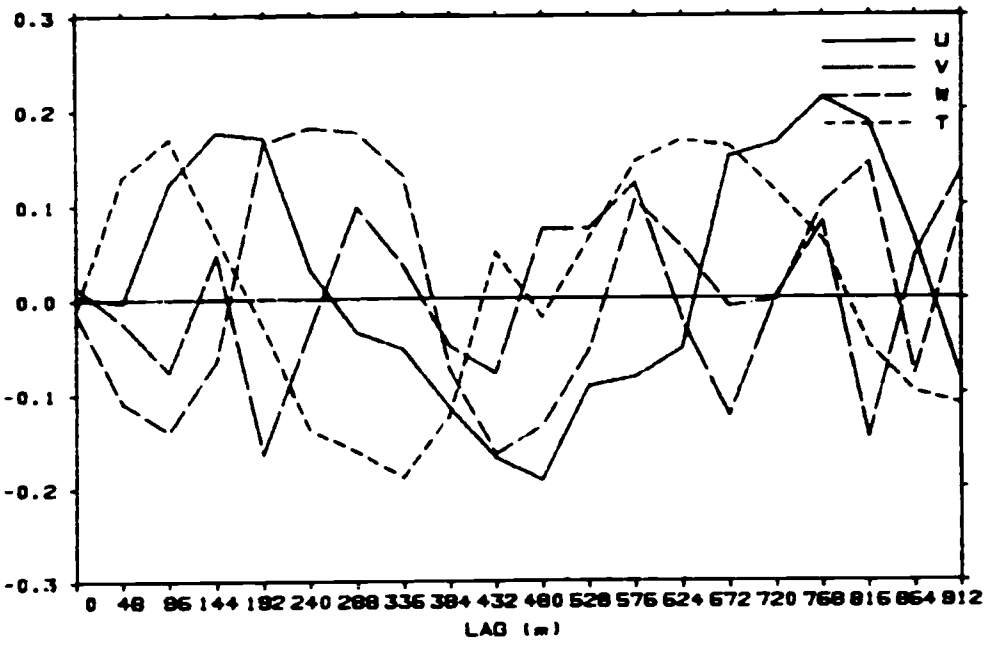


(a)

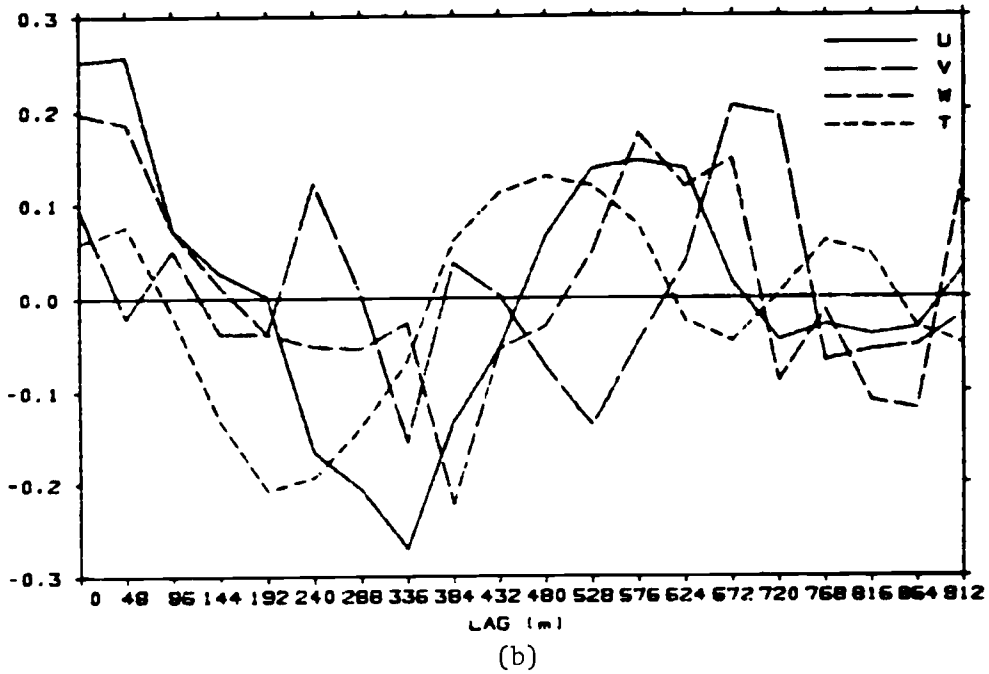


(b)

Fig.A4: First (a) and second (b) eigenvectors for continuous weighting for leg XW.

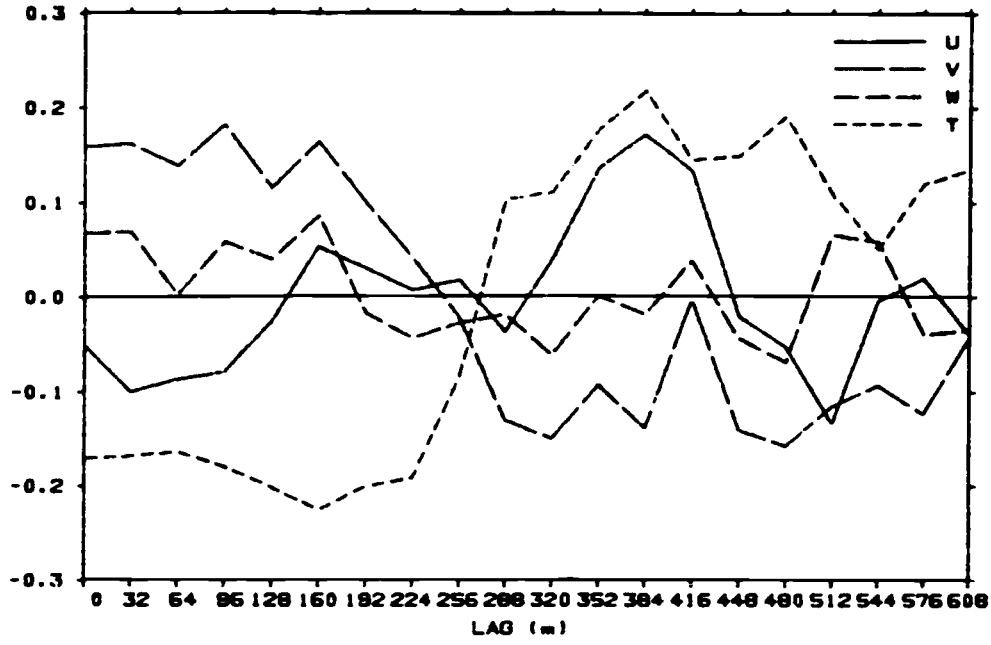


(a)

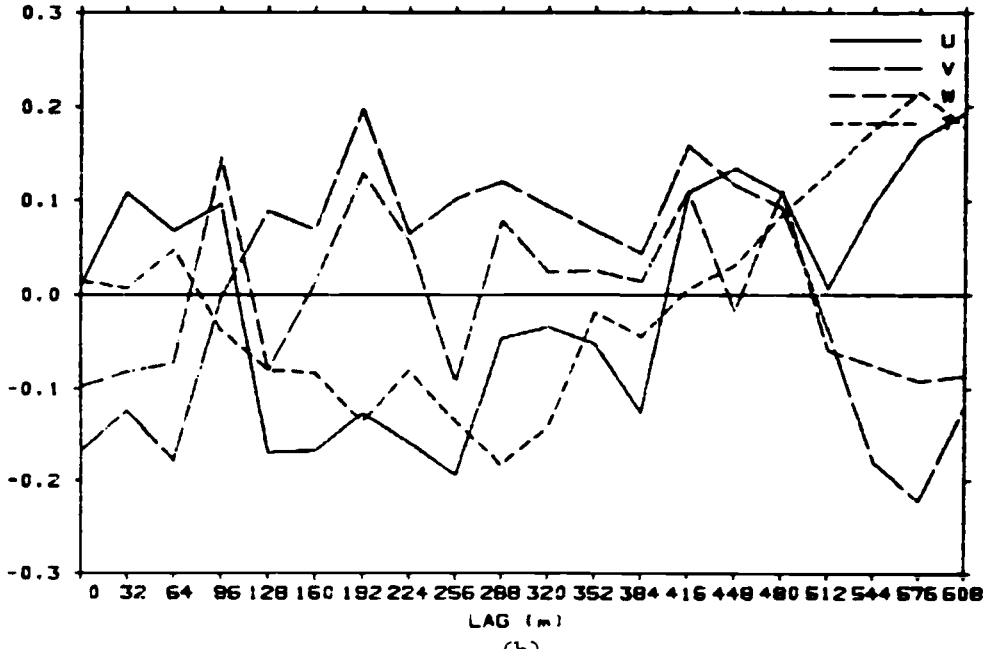


(b)

Fig.A5: First (a) and second (b) eigenvectors for conditional sampling for SESAME, 6 May.

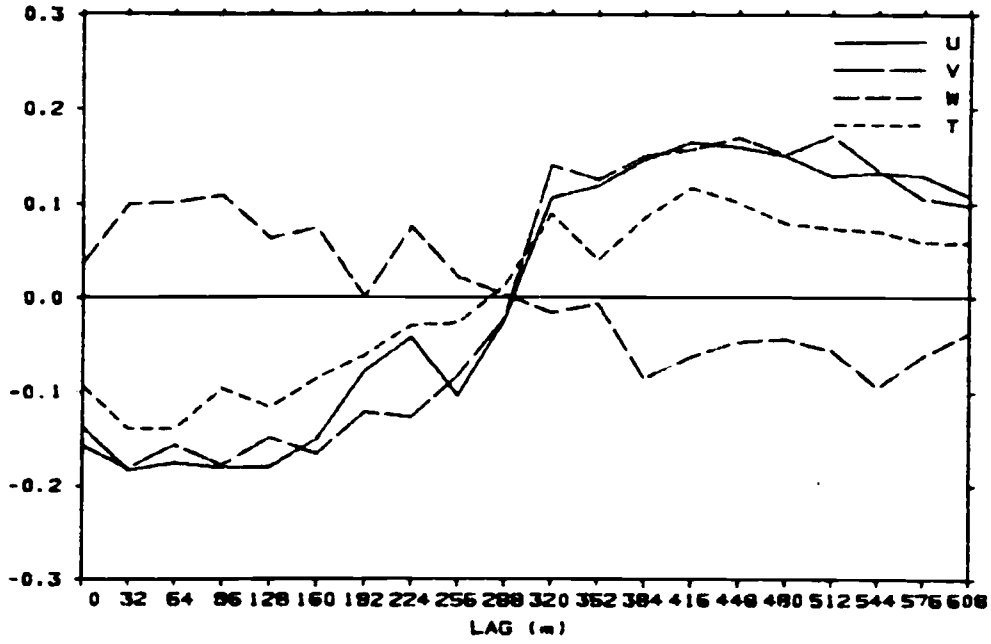


(a)

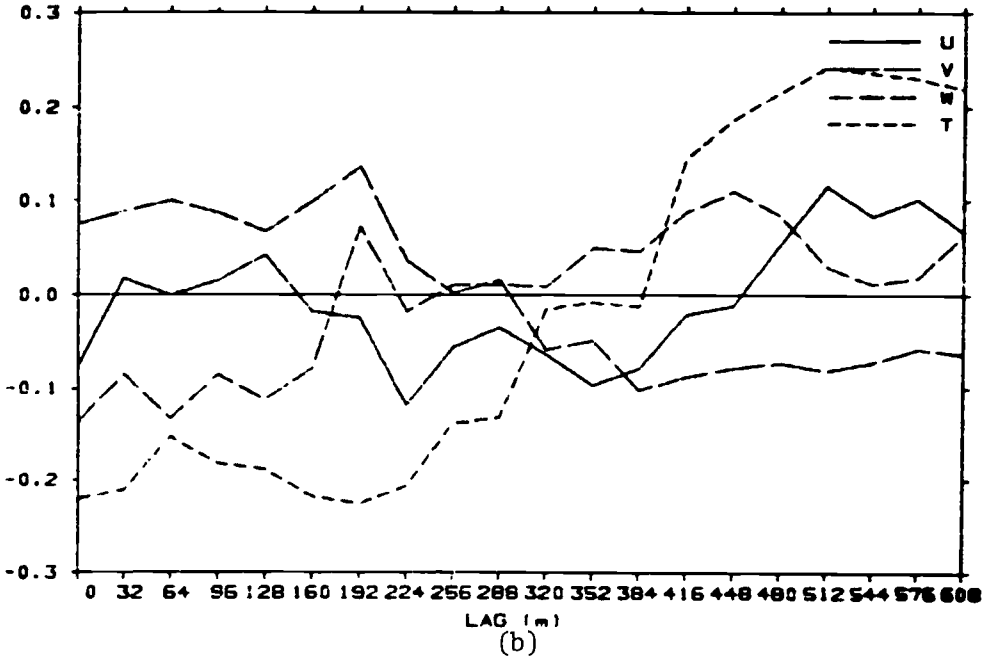


(b)

Fig.A6: First (a) and second (b) eigenvectors for conditional sampling for SESAME, 5 May.

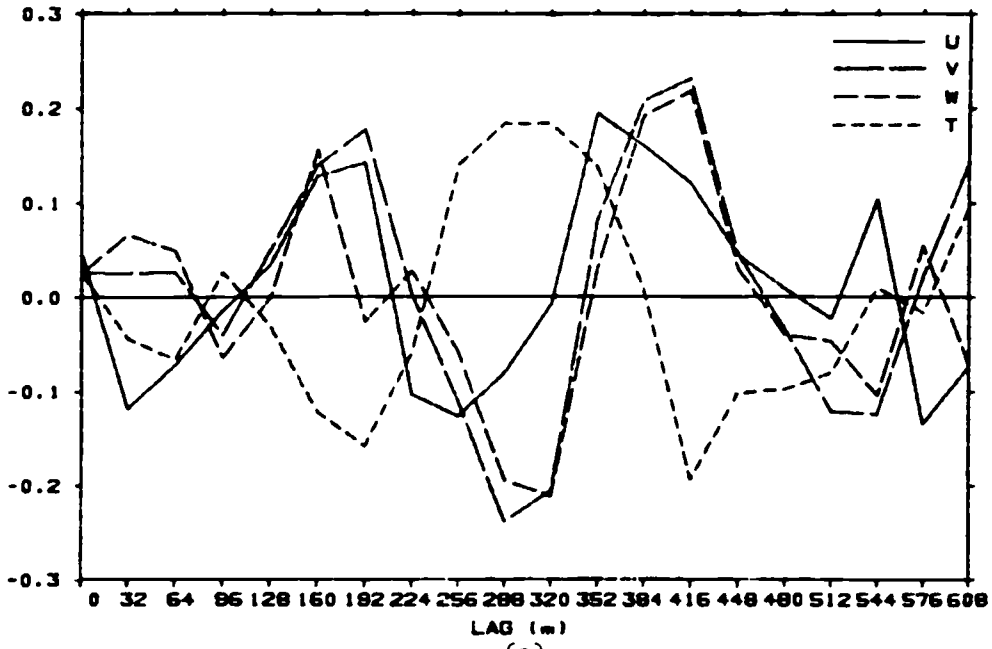


(a)

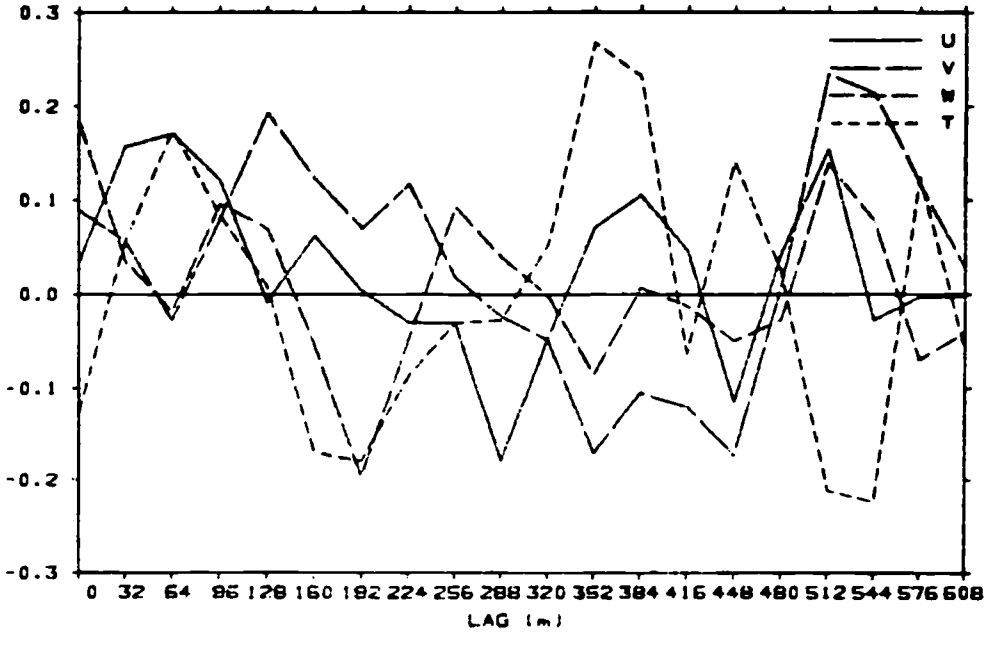


(b)

Fig.A7: First (a) and second (b) eigenvectors for continuous weighting for SESAME, 6 May.

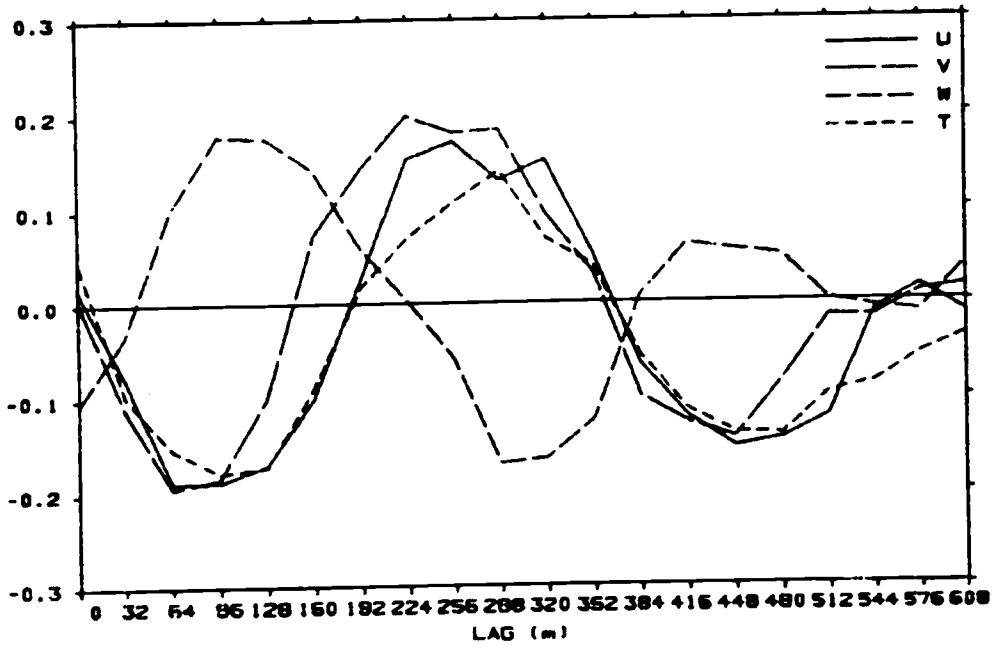


(a)

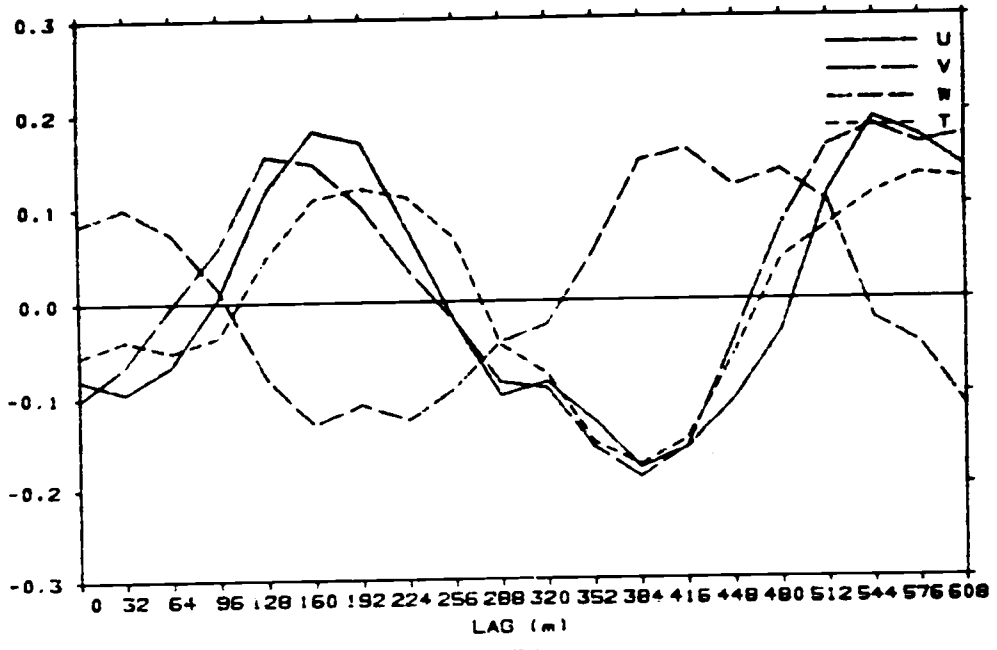


(b)

Fig.A8: First (a) and second (b) eigenvectors for continuous weighting for SESAME, 5 May.